國立臺灣大學理學院大氣科學研究所

碩士論文

Department of Atmospheric Sciences

College of Science

National Taiwan University

Master Thesis

物理和化學作用對 NO_x 日變化影響之理想模擬研究

Physical and Chemical Effects of Diurnal Evolution of NO_x Concentration in Idealized Simulations

范祐軒

Yu-Hsuan Fan

指導教授：吳健銘 博士

Advisor: Chien-Ming Wu, Ph.D.

中華民國 111 年 6 月

June, 2022

doi:10.6342/NTU202201146

謝辭

回想踏上研究的道路上，從大四的時候沒什麼方向，就去找吳健銘老師說要做獨立研究，心裡想的只有想做有關於空氣汙染的研究模擬，不過在老師的建議下，先熟悉了模式的設定和模擬，從比較簡單的海陸風分析來練習，慢慢地學到了做研究的方法。而後有幸考上了研究所，終於能進行最初想做的空氣汙染傳送的模擬，但在過程中卻遇到了不少問題，有時候是想看的問題太廣無法聚焦，有時候則是會卡在特定問題上無法解決，很感謝吳健銘老師在我迷失方向時幫忙一起解決問題，和老師討論時常常都會被一語點醒，不論是研究上或是人生方向上的建議都讓我獲益良多。每個學期的 Group meeting 報告，也感謝陳維婷老師提出關鍵的問題，讓我重新思考我的研究，補足研究上的缺失。此外還要感謝洪惠敏老師，儘管繁忙之中還是願意和我進行研究的討論，幫助我精進研究中化學的部分。

而在 C302.5 研究室的生活中，首先感謝金德學長幫助我解決模式上的所有問題，從 VVM 的熟悉到化學模組和傳送 budget 分析，都願意在忙碌之中抽出時間和我一起 debug。在平常遇到各式各樣的問題，很感謝宇泓學長都願意聆聽我的疑問並且給予解答，以及在準備報告上給予不少幫助。針對我的研究，感謝同在進行空汙研究的旻耕學長和子涵學姐給了不少建議。下午累的時候，感謝啟桓、宗育、少禹、乃文同居的大家以及實驗室的所有人一起吃東西聊天，放鬆心情。課外之餘，感謝吉哥、淳弘和系壘的大家讓我在研究外能夠有運動紓解壓力的機會，和大家一起打球的感覺非常快樂。此外，還要感謝 B05 的同學們，為我的研究生活增添不少樂趣，像是一起吃飯、唱歌、看球等等，讓這充滿疫情的日子裡精彩了不少。最後要感謝我的家人，讓我不用煩惱經濟上的問題，無時無刻都給予我最大的支持，壓力大的時候一起聊天紓解，遇到問題時一起討論解決，有了大家的幫忙，我才能完成這個研究。

doi:10.6342/NTU202201146

摘要

本研究旨在利用海洋、陸地和山脈分布的理想模擬，研究局部排放的日變化所受到的物理和化學作用。在台灣冬季弱綜觀的天氣型態下，由於局部環流和複雜地形之間的相互作用，很難評估局部排放如何影響空氣品質，因此本研究使用與化學模組耦合的三維渦度向量方程雲解析模式 (VVM) 進行理想化模擬，以釐清物理和化學過程對局部排放的影響。化學方面僅使用兩個反應將複雜的化學交互作用簡化為保守的化學系統，實驗中主要針對兩種排放源，分別是廣泛分佈在城市平原地區的交通排放，以及在狹長沿海工業區的高濃度工業污染排放，排放量則根據台灣的歷史空氣汙染排放數據 (臺灣空氣污染物排放量清冊, TEDS) 。在平原地區，交通排放在清晨累積在地表附近，但在邊界層形成後，污染物濃度受到垂直混合被稀釋。另一方面，工業排放的汙染傳送主要為海風控制，在下午隨著海風前緣進入內陸地區，影響內陸地區的空氣品質。在山區，兩種排放源的汙染物皆由海風傳送主導，於傍晚從平原地區被海風傳送到山區。因此，我們可以在平原地區觀察到兩個汙染濃度峰值，而在山區只有一個濃度峰值。再者可以利用停留時間的機率分布來分析不同汙染源在時間上的表現，由此可知工業排放主要停留在五百公尺以下的平原地區，而交通排放則在邊界層頂累積並維持較長的時間。此外，白天氮氧化物之間的轉換以光解反應為主，可以觀察到臭氧的增加，而排放的一氧化氮和二氧化氮比率在影響化學平衡中也扮演重要的角色。在夜間，一氧化氮和臭氧反應生成二氧化氮，二氧化氮是二次氣溶膠的前驅物，經歷夜間反應後可能會導致山區污染。由於不利汙染散布的氣象條件和過多的氮氧化物排放，平原地區的臭氧在第二天晚上耗盡。此研究得知釐清物理過程以了解污染物濃度的局部變化的重要性，持續的汙染排放和化學作用則造成一氧化氮和二氧化氮的比率在兩天之間發生劇烈變化。

關鍵字：汙染傳送、大渦流模擬、海風環流、邊界層過程、氮氧化物反應

doi:10.6342/NTU202201146

Abstract

This study aims to investigate the diurnal evolution of local emissions based on the physical and chemical views in idealized simulations with ocean, land, and mountain distribution. During the wintertime weak synoptic condition in Taiwan, it is difficult to evaluate how local emissions influence the air quality due to interactions between the local circulation and complex topography. Idealized simulations using the Vector Vorticity equation cloud-resolving Model (VVM) coupled to a chemistry parameterization are performed to study the impacts of physical and chemical processes on local emissions. Two nitrogen reactions are applied to simplify the chemical interactions to a conservative chemical system, and the local emissions are based on historical air pollution data in Taiwan (Taiwan Emission Data System, TEDS). The traffic emissions are broadly distributed over urban plain areas, while high-concentration industrial pollutants are emitted in very limited coastal areas. Over the plain areas, traffic emissions accumulated in the early morning, but the concentration of the pollutants was diluted through vertical mixing after the boundary layer developed. On the other hand, the transport of industrial emissions is controlled by the sea breeze, and highly polluted air is transported with the sea breeze front invading inland regions in the afternoon. In the mountain areas, both emissions are transported by the sea breeze from the plain areas in the evening. Thus, we can observe two concentration peaks over

doi:10.6342/NTU202201146

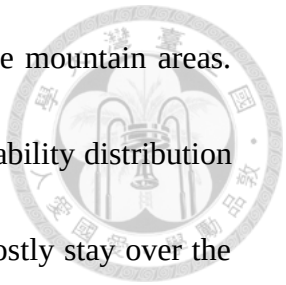

the plain areas, while there is only one concentration peak over the mountain areas. Another aspect of physical effects could be analyzed using the probability distribution of the residence time, which shows that the industrial emissions mostly stay over the plain areas under 500m, while the traffic emissions accumulated at the boundary layer top and persist for an extended period. Besides, the transformation between NO_x in the daytime is dominated by photodissociation; an increase in O_3 can be observed in the daytime, while the emitted NO/NO_2 ratio also plays an important role in affecting chemical equilibrium. During the nighttime, NO and O_3 react to produce NO_2, which is the precursor of secondary aerosols that would lead to a polluted condition in the mountain areas. Due to unfavorable meteorological conditions and excessive NO_x emissions, O_3 runs out on day 2 evening over the plain regions. The results highlight the importance of resolving the physical processes to understand the local evolution of pollutant concentration. Excessive emissions and the effect of chemical reactions lead to a drastic change in the NO/NO_2 ratio between day 1 and day 2.

Keywords: pollution transport, large eddy simulation, sea breeze circulation, boundary layer process, NO_x reactions

doi:10.6342/NTU202201146

Contents

doi:10.6342/NTU202201146

Figure captions

doi:10.6342/NTU202201146

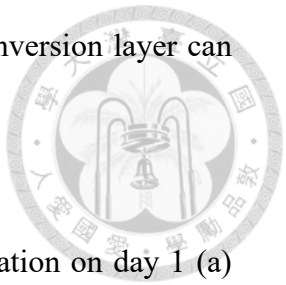

doi:10.6342/NTU202201146

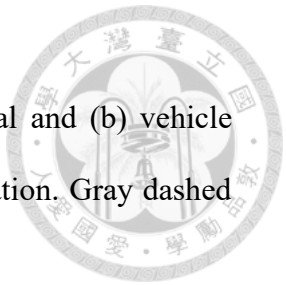

doi:10.6342/NTU202201146

Table captions

doi:10.6342/NTU202201146

1 Introduction

Air pollution is one of the biggest public health hazards worldwide. According to the WHO estimates in 2016, ambient air pollution in both cities and rural areas was estimated to cause 4.2 million premature deaths per year globally, and the evidence linking the ambient air pollution and the cardiovascular disease risk is growing (The Multi-Ethnic Study of Atherosclerosis and Air Pollution). In the past decade, several studies have pointed out an association between ambient air pollution and mortality from respiratory and cardiovascular diseases in Taiwan (Liang et al., 2009; Tsai et al., 2010). Further research also showed that ambient air pollution was associated with an incidence of headache, incident asthma, lung cancer, and colorectal cancer (Chiu et al., 2015; Jung et al., 2019; Tseng et al., 2019; Ma et al., 2020). Since air pollution is a serious public health concern, it is essential to understand the transport of air pollution to control and reduce air pollution emissions.

The air pollution problem in central Taiwan is a critical environmental issue. The cause of air pollution in Taichung has been a debated issue in recent years. The biggest core-fired power plant in Taiwan; Taichung Power Plant, is usually to blame for worsening air quality in central Taiwan. Previous study showed that $PM_{2.5}$-related health risks were associated with the emissions from Taichung Power Plant (Kuo et al., 2014). According to the Taiwan Emission Data System (TEDS) from Environmental Protection

doi:10.6342/NTU202201146

Administration (EPA), there were 22026 MT/yr of NO_x and 15179 MT/yr of SO_x emitted by Taichung Power Plant in 2016, which is the most significant pollution source in Taichung. However, emissions by Taichung Power Plant had drastically decreased in 2019, only accounting for 9844 MT/yr of NO_x and 8224 MT/yr of SO_x. Besides, people tend to ignore vehicle emissions in urban areas, which is another major emission source. In 2019, the largest NO_x emission in Taichung came from vehicle emissions, which made up almost half of the total NO_x emission in Taichung, accounting for 17155 MT/yr. It is worth knowing which emission is more critical for damaging local air quality to prevent and control air pollution in the future.

In Taiwan, air pollution events usually happen in the winter and spring (Hsu & Cheng, 2019; Hsu, 2021). Transport and dispersion of air pollutants are closely associated with meteorological conditions; for example, synoptic weather pattern plays a vital role in controlling the distribution of air pollutants (Cheng, 2001). Under a stable environment in the lower troposphere, low wind speed and low mixed layer height can also lead to highly polluted events (Yu & Chang, 2006; Su et al., 2020). Previous studies also focus on the air pollution problem in central Taiwan, they investigated that under a weather condition characterized by low wind speed and a shallow mixed layer depth capped by a strong inversion, local circulation, and regional orography are key factors influencing pollution concentration (Cheng et al., 2001; Cheng, 2002). Hsieh et al. (2022) also found

doi:10.6342/NTU202201146

that local circulation under different meteorological conditions coupled with the evolution of boundary layer can induce contrasting pollution transport scenarios. Since many meteorological processes and chemical interactions have different impacts on the transport and dispersion of air pollutants, one of the emission sources might be the key factor that accounts for higher pollutant concentrations in the downwind areas.

In Taiwan, over 70 air quality monitoring stations are installed by EPA to monitor air quality. However, using actual observation data to analyze transport and dispersion of air pollution still encounters some obstacles. Since many physical and chemical effects are involved in the transport and dispersion of air pollutants, such as local circulation, cloud dynamics, boundary layer processes, topography, dilution, and deposition. Sometimes it is quite difficult to make a clear distinction between these effects, especially when the time evolution of air pollutants from real observation is diagnosed from scattered stations. However, with a LES model based on appropriate physical and chemical processes, we can simulate the transport and dispersion processes directly, and thus provide a precise interpretation of those effects.

Over the past decades, large eddy simulation (LES) has evolved into one of the major techniques for simulating transport processes in the atmospheric boundary layer (Garratt, 1994). Using high resolution and appropriate dynamic schemes, LES can simulate complex flows and turbulence structures, given more specific details of boundary layer

doi:10.6342/NTU202201146

development and its impacts on transport processes. In atmospheric chemistry, different compounds interact with each other and create a complex chemical system. Reactions can change the composition of the pollution and then affect local air quality in different areas during pollution transport processes. Moreover, several reactions are greatly influenced by meteorological conditions; for example, sunlight has a dominant effect on photodissociation, which shows that the presence of clouds is also an important factor controlling photodissociation.

Section 2 introduces model description and an implementation of the chemistry module with a supporting comparison test. Section 3 provides meteorological conditions that we are interested in and the experiment setup for our idealized simulation. Section 4 shows the results of our idealized simulation. Section 5 is the summary and discussion.

doi:10.6342/NTU202201146

2 Model Description and Evaluation

2.1 Vector-Vorticity Equation Cloud-Resolving Model (VVM) introduction

The model here we use is Vector Vorticity equation cloud-resolving Model (VVM), developed by Jung and Arakawa (2008) and Wu et al. (2019) based on the three-dimensional anelastic vorticity equations. The model predicts the horizontal components of vorticity and diagnoses the vertical velocity using a three-dimensional elliptic equation. This unique method can simulate local-scaled circulations and land-sea breezes due to sharp responses to the local buoyancy gradient. To deal with topography, Wu and Arakawa (2011) and Chien and Wu (2016) applied an immersed boundary method with the topography forcing added to the vorticity fields in height coordinate, which can resolve complex and steep terrain without computation problems. Improving the conception of land-atmospheric interactions over complex topography, Wu et al. (2019) coupled the Noah LSM version 3.4.1 (Chen et al., 1996; Chen & Dudhia, 2001) to VVM to provide a more realistic representation of land surface properties as well as surface fluxes. VVM has been used for studying complicated interactions, such as the unified parameterization of deep convection (Arakawa & Wu, 2013; Wu & Arakawa, 2014), stratocumulus transition (Tsai & Wu, 2016), the aggregated deep convection (Tsai & Wu, 2017), afternoon thunderstorms (Kuo & Wu, 2019), land-atmosphere interactions (Wu et al., 2015; Wu et al., 2019; Wu & Chen, 2021), cloud-aerosol interactions (Chang et al.,

doi:10.6342/NTU202201146

2021), the coastal convection during summer monsoon onset (Chen et al., 2019), convective aggregation (Huang & Wu, 2022), and tracer transport (Hsieh et al., 2022).

2.2 Implementation of Chemistry Module

The transport and dispersion processes of pollutants involve not only physical effects but also chemical effects. Thus, chemical reactions between different chemical components should be considered in the simulations. To construct an atmospheric chemistry system in VVM, the chemistry module is implemented into VVM following Dutch Atmospheric Large-Eddy Simulation (DALES). This module has been tested and applied to the research for photodissociation and turbulent reacting flows (Vilà-Guerau de Arellano et al., 2005; Vilà-Guerau de Arellano et al., 2009; Heus et al., 2010). The chemistry module can be roughly divided into the initiation stage and the chemical solver (called "TWOSTEP") stage. In the initiation stage, chemical mechanisms and related parameters are input into the module. Unlike DALES, the initial fields and emission sources in VVM are arranged into a module. After initializing the model and finishing the calculation of dynamics, chemical reactions are solved using the chemical solver TWOSTEP described and tested by Verwer (1994) and Verwer and Simpson (1995). First, the module needs to deal with the reaction rates under different environmental conditions. Since chemical reactions depend on meteorological parameters, such as pressure,

doi:10.6342/NTU202201146

temperature, and liquid water content, essential meteorological data will be input into the module when calculating the reaction rates. When calculating the concentration of chemical components, the solver uses an implicit method based on the variable-step, second-order backward differentiation formula. Since the atmospheric chemistry system is characterized by a wide range of chemical time scales, the solver can adjust the time step depending on different chemical reaction rates in the model. When the calculation of the new chemistry time step is the same as the next model time step, the model can advance to the next model time step and calculate the dynamics. By using this chemistry module, the chemistry system can be simulated, and chemical effects on the transport and dispersion of air pollutants can be further investigated.

2.3 Diurnal cycle of shallow convection over land

To check the suitability of the chemistry module in VVM, a shallow convection simulation was demonstrated following Vilà-Guerau de Arellano et al. (2005, hereafter V05). The experiment setup is described as follows. The model domain size is 6400 by 6400 m^2 horizontally with a grid length of 66.7 m. In the vertical, the domain height is 4000 m with a grid length of 40 m. Initial profiles of potential temperature, specific humidity, and surface fluxes follow Brown et al. (2002) representing a typical shallow convection over land, which show in Fig1. The case is characterized by a strong diurnal

doi:10.6342/NTU202201146

cycle of both sensible and latent heat fluxes. The formation of shallow convections is induced by these large surface forcings. The simulation is integrated from 05:30 LT to 18:30 LT. The chemical system is based on a simple atmospheric cycle of nitrogen dioxide, nitric oxide, and ozone, including two reactions:

$$NO_2 + O_2 + h\nu \xrightarrow{j} NO + O_3 \quad (1)$$

$$NO + O_3 \xrightarrow{k} NO_2 + O_2 \quad (2)$$

where j and k are first-order photolysis rate and second-order chemical reaction rate. Following the setting in V05, the surface fluxes showed in Table 1, $j=8.3\times10^{-3}$ (s^{-1}) and $k=4.75\times10^{-4}$ (ppb s^{-1}) are fixed with time in the simulation to reach chemical equilibrium quickly. The initial mixing ratio profiles of chemical species also follow V05 which show in Fig. 1 (c).

2.4 Results of Comparison Test

To clarify the physics and dynamics processes of the simulation, we analyze the model outputs shown in Fig. 2 and Fig. 3. Cloud fraction begins to grow after 9:30 LT with a small liquid water path, referring to a relatively thin cloud in development. At 11:30 LT, a well-mixed layer can be observed in Fig. 2. The cloud layer above the well-mixed boundary layer didn't reach conditionally unstable yet, and there is an absolutely stable boundary layer above the cloud top. After 12:30 LT, the cloud fraction reaches the

doi:10.6342/NTU202201146

maximum value of the simulation, coupling with a cloud top height of 1.5 km and a cloud layer thickness of around 1 km. This three-layer structure is maintained at 14:30 LT, and the clouds have matured. Since the surface fluxes quickly decline after 16:00 LT, the cloud fraction and liquid water path drop around 16:30 LT, and the clouds finally disperse at 18:00 LT. Compared to the results from V05, the two models both predict similar boundary layer evolution; however, the well-mixed layer height in VVM is slightly lower than that in DALES, which indicates that the boundary layer development is slower in VVM. For cloud properties, VVM can provide a daily evolution of shallow cumulus over the land like DALES. But the cloud top height and cloud base height in VVM are lower than those in DALES, and liquid water path in VVM are larger than those in DALES. These differences slightly affect the performance of the chemical system between VVM and DALES simulations.

The performance of chemical reactions can be observed by the mean profiles of chemical reactants shown in Fig. 4. At 8:30 LT, the reactants and inert scalar accumulate at the surface layer before boundary layer development. After 11:30 LT, it is clear that those tracers mix vertically, resulting from the growth of the boundary layer. At 17:30 LT, a two-mode structure can be observed in all four tracers, which might be associated with the enhancement of the transport in the cloud. Compared to the results from V05, we notice that the boundary layer height in VVM is lower than that in DALES, which is

doi:10.6342/NTU202201146

consistent with the results from the previous physical part. Furthermore, the concentration of the three reactants has minor differences between the two models. Since cloud top height and liquid water path in VVM have some differences from those in DALES, we guess that high liquid water coupled with lower clouds lead to a weaker total photolysis rate, resulting in a higher nitrogen dioxide concentration and a lower nitric oxide and ozone concentration, which is relatively apparent at 17:30 LT. In the end, both the performances of physical processes and chemical reactions in VVM are similar to the results from DALES. Through the comparison, we think that the chemistry module in VVM can work successfully and reasonably; therefore, we can start to run our idealized simulations to figure out the physical and chemical effects of air pollutants in central Taiwan.

doi:10.6342/NTU202201146

3 Idealized Experiment

Our idealized experiment aims to figure out the physical and chemical effects of different NO_x pollution sources in central Taiwan. To focus only on the effects, we try to simplify the land-sea structure in central Taiwan to avoid complicated mountain wave turbulence. An arrangement of ocean, land, and mountain is applied to the experiment; the ocean region is equal to the land region. The land region is separated into two areas of the same size: a flat plain and a 1000m-high mountain shown in Fig. 5. Land use is also simplified, referring to the data from Noah LSM, urban and built-up land is set in plain regions, and the evergreen broadleaf forest is set in mountain regions. The simulation is set to run for two days with a different purpose. Since only ozone has been set at the initial concentration, the concentration of NO_x is controlled by the emission sources and pollution transport. On day 1, it is direct and applicable to analyze physical and chemical effects without the influence of background concentration in real observation. On day 2, because deposition and dissipation are not set in the simulation, the emitted NO_x on day 1 will remain and be sketchily represented as background concentration. The transport pattern of day 2 might be similar to the pollution transport in reality. We expect that industrial emissions along with the coastal areas and vehicle emissions in the urban areas will have different patterns of transport and dispersion. Under a sea breeze-dominated environment capped by a strong inversion, low wind speed

doi:10.6342/NTU202201146

and suppressed mixed layer depth are the important factors affecting pollution transport.

3.1 Idealization of boundary layer process in Taiwan

In Taiwan, the boundary layer process is a key factor associated with pollution transport. In summer, warm weather conditions coupled with strong surface fluxes build a favorable environment for boundary layer development; the atmosphere is heated by the increasing surface temperature, which induces vertical motion and the mixing process. Near-surface pollution can be transported vertically through mixed layer development, and the concentration of pollutants can also decrease due to vertical mixing. Thus, few air pollution events are related to the boundary layer process in the summertime. However, the boundary layer process can cause different consequences in wintertime. The mixed layer can develop in the daytime due to surface fluxes. Yet, the cold weather condition is an unfavorable factor for the growth of mixed layer height, and sometimes the development is inhibited by an inversion layer, resulting in a relatively low mixed layer height compared to summertime. Air pollution can still be diluted by vertical mixing when the mixed layer grows; while dispersion is limited, most pollutants remain near the surface. Since pollution is trapped near the surface, it is difficult to transport through vertical mixing or prevailing winds. Pollutants tend to be accumulated and cause serious pollution events. At night, mixed layer height drops, and air pollution further concentrates

doi:10.6342/NTU202201146

near the surface, extending the period of severe pollution events. In sum, the boundary layer process is one of the major meteorological factors in influencing the transport and dispersion of air pollutants and causing air pollution events in winter.

3.2 Idealization of local circulation in Taiwan

Local circulations also play an important role in pollution transport in Taiwan. Many industrial parks are located in the coastal regions of Taiwan. Once the weather condition is dominated by local circulation such as the land-sea breeze, air pollution emitted by the industries can particularly affect the air quality of downwind areas. Before the onset of sea breezes, air pollution emitted in the industrial parks can only diffuse near the emission sources or be transported vertically through the mixing process. When the sea breeze is induced by the difference between the temperature of land and sea, air pollution along coastal regions is expected to invade inland regions with the sea breeze. Due to steep mountainous terrain in inland regions, the sea breeze cannot penetrate further, leading to an accumulation of pollutants at the foothill. At night, sea breezes will be shifted into land breezes; however, the strength of land breezes is relatively small and can't extend to inland regions. The pollutants transported by sea breezes might remain in inland regions for a longer period. Over mountain regions, the mountain-valley breeze can play a similar role in air pollution transport as the land-sea breeze. In the daytime, valley breezes

doi:10.6342/NTU202201146

transport urban air pollution from foothills into mountain areas, causing poor air quality conditions over mountain regions.

3.3 Experiment setup (from physical to chemical setup)

The horizontal model domain covers 256km times 16km with a grid spacing of 250 m and doubly periodic boundary conditions as shown in Fig. 5. The domain setup forces the transport along the x-axis to clarify the impacts of pollution transport from local circulation. There are 100 vertical layers, and the resolution is 50m. We run the model for 2 days, starting at 12 am local time. The scenario of two consecutive days followed Hsu (2021), which emphasized pollution accumulation on Day 2 due to unfavorable meteorological conditions for pollution transport. Our idealized weak synoptic weather condition is characterized by weak wind speed and shallow mixed layer height capped by a temperature inversion layer. The initial potential temperature and water vapor mixing ratio profiles are shown in Fig. 6 following Hsieh et al. (2022), which contain a temperature inversion layer. To focus on a local circulation-dominated weather type with low wind speed, we set the prevailing winds to zero. The chemical system is based on the atmospheric cycle of nitrogen dioxide, nitric oxide, and ozone, including two reactions that are the same as that we used in the comparison test. By using a simple chemical system, the influence of meteorological conditions on the transport of pollution can be

doi:10.6342/NTU202201146

determined. For the chemical condition, to get closer to observation, the initial ozone is given at 40 ppb, representing an average amount in the typical winter condition in Taiwan. There are three NO_x emission scenarios in our idealized simulation. The first two emission scenarios are two main emission sources that affect the air pollution in central Taiwan, same as in section 1, all-day industrial emission in coastal areas and daytime traffic emission in urban areas. The specific set of these two emission sources is shown in Table 2. The last emission scenario considers both industrial and vehicle emissions, representing the total NO_x emission in central Taiwan. Taiwan emission database system version 11.0 (TEDS 11.0) based on 2019 in Taichung is used as our dataset. For NO_x emission, the emitted NO/NO_2 ratio is assumed to be 9:1, following Lien and Hung (2021).

doi:10.6342/NTU202201146

4 Results

4.1 Physical effects of total emissions

There are two main physical factors. The first one is boundary layer processes, which control the vertical transport of pollutants; and the second one is local circulation, such as sea breeze, which mainly dominates the horizontal transport of pollutants. Owing to a simplified chemical system based on the photodissociation of nitrogen dioxide and a reaction of nitric oxide and ozone, using the NO_x profile can eliminate chemical effects and clarify the physical effects in our simulation. First, LES can simulate boundary layer processes and local circulation structures distinctly; therefore, pollution transport affected by these effects can be clarified through cross-section profiles in the x-z plane. In Fig. 7, it is clear that pollution transport is affected by vertical mixing in plain regions in the morning and sea breezes from coastal to inland and mountain regions in the afternoon. The evolution of the vertical profiles of NO_x concentration in different regions over land is demonstrated in Fig. 8. All profiles show the growth of the boundary layer and vertical mixing of concentration during the day. At 17:00, there is a decrease in the concentration over the coastal region at 500m, which is associated with clean marine air transported by the sea breeze.

The concentration c of chemical species i is governed by the transport equation,

$$\frac{\partial c}{\partial t} = -\vec{u} \cdot \nabla c - \mathrm{D}\nabla^2 c + E + (P_i - L_i) \quad (3)$$

doi:10.6342/NTU202201146

which neglects sink term. The four terms on the right side of the equation represent advection, diffusion, emission, and chemical production and loss, respectively. To clarify the process resulting in a drastic concentration change, we show the time evolution of NO_x concentration, sea breeze strength, boundary layer height, and the budget of transport equation at the surface in Fig. 9 & 10. Since the model output frequency is 10 minutes, the unit in the transport equation is parts per billion (ppb) per 10 minutes. In Fig. 9, the change of concentration of NO_x follows a diurnal evolution with two peaks per day. The first peak happens around 8:00, which is associated with low wind speed and low boundary layer height; therefore, continuous emissions after the sunrise couple with an unfavorable condition for air pollution transport resulting in the first peak of NO_x concentration. Another peak can be observed in the afternoon, which is associated with the maximum value of sea breeze. Hence the second peak is contributed by the air pollution transport of sea breeze. The contribution of the variation of NO_x concentration can be quantified by the budget of transport equation in Fig. 10. After 6:30, A large increase in NO_x concentration of 6.5 ppb/10mins is caused by emission of 11.5 ppb/10mins at the surface. However, diffusion also increases to remove NO_x concentration from surface to upper atmosphere and reaches a maximum of -24.2 ppb/10mins around 8:30, resulting in a sharp decrease in NO_x concentration of -12.8 ppb/10mins. In addition, the urban plain region is covered with traffic emissions after

doi:10.6342/NTU202201146

sunrise, and the diffusion is forced in the only vertical direction. The influence of advection appears around 10:00, causing another sharp decrease in NO_x concentration, while the amount of -6.9 ppb/10mins is less than that from the influence of diffusion. At 16:00, an increase in NO_x concentration can be observed and is associated with an increase in advection, which is mainly contributed by the advection of 16.8 ppb/10mins, with a significant positive horizontal advection term of 26.7 ppb/10mins and a negative vertical advection term of -9.9 ppb/10mins. Apart from a positive peak of advection term during sea breeze invasion, total advection is negative in most of the moment, which leads to a decrease in NO_x concentration. In Fig. 11, extreme values and the peak times of advection and diffusion are analyzed and shown in two days. Since the plain areas are filled with traffic emissions from the surface, the analysis of diffusion is only focused on the vertical direction. The largest advection is found at the coastlines, which is produced by the industrial emission and the effect of sea breezes, and the advection decreases from coastal regions to inland regions. The maximum advection in coastlines is four times larger than over inland regions. On the other hand, both peak values and the peak times of vertical diffusion are almost the same in plain regions since the traffic emission sources are equally distributed. The impact of vertical diffusion plays an important role in plain regions. The order of magnitude of vertical diffusion is the same as that of total advection at the surface level, which indicates that turbulences in the mixed layer mainly govern the

doi:10.6342/NTU202201146

vertical transport of traffic emission at the surface. In mountain regions, change of concentration is controlled primarily by the contribution of advection, and maximum advection exceeds 20 ppb/10mins, which is associated with the pollution transport of sea breeze.

4.2 Differences between physical effects of industrial and vehicle emission

Two scenarios of industrial and vehicle emission sources are simulated separately, so we can analyze the physical effects of each emission source individually. First, we focused on industrial emissions in Fig. 12 (a). It is clear that polluted air accumulated at the coastlines in the morning. After sea breezes onset at 12:00, NO_x pollution starts to move with sea breezes into inland regions, with a wind speed of 2.5 m/s. Around 16:00, the NO_x concentration around the coastal region drops, and sea breezes bring clean marine air into the coastal region, indicating that surface pollution along the coast has been transported into the inland region. In inland and mountain regions, NO_x pollution transported by sea breezes arrives in the evening. NO_x pollution is difficult to diffuse because the boundary layer drops at night. On day 2, the transport pattern doesn't change a lot, and we can see a higher concentration due to the accumulation of two days.

On the other hand, vehicle emissions showed another transport pattern seen in Fig. 12 (b). In the early morning of day 1, severe air pollution accumulates over plain areas

doi:10.6342/NTU202201146

before boundary layer development. After 8:30, the boundary layer started to grow, and the concentration of pollutants decreases. From 10:00 to 13:00, vehicle emission is transported away from the surface through vertical mixing. The concentration of pollutants is relatively low at the surface compared to early morning. While sea breezes flow into land and tend to gather vehicle pollution from the coast to inland in the afternoon, concentration gradients can be observed in plain regions. Descent of boundary layer height also contributes to the accumulation of pollutants; thus, a local maximum of pollutants appears at the foothill. As the same as industrial emission, the transport pattern of vehicle emission doesn't change much on day 2, but the accumulation on day 1 is evident.

In Fig. 13, maximum concentrations and peak times are analyzed and shown in two days, with two emission sources. Maximum concentrations of industrial NO_x decrease from coastal to inland areas, and peak times match with arrival times of sea breeze. There are few differences between the two days. While maximum concentrations of vehicle NO_x are almost the same in plain regions, they all occur in the early morning. Maximum concentrations of vehicle NO_x slightly increase over inland regions, which is associated with the accumulation effect of sea breeze. In mountain regions, both industrial and vehicle NO_x show similar performances of peak time and the change of concentration between the two days.

doi:10.6342/NTU202201146

Another aspect showing the physical effects of pollution emissions can be seen in the probability density function of duration in Fig. 14. The concentration of NO_x larger than 10 ppb is chosen as the criterion. A larger number represents that the place has been polluted for a longer duration. It is clear that industrial emissions in the left figure mostly stay in the land regions under 500m. Vertical mixing has little impact on the transport of industrial emissions. The sea breeze is an important pathway for transporting industrial emissions into inland regions. In contrast, vehicle emissions are stuck at the boundary layer top for a long period, which is contributed by the boundary layer processes. Another polluted area of vehicle emission is observed at the foothill, which might be related to the accumulation induced by sea breezes.

4.3 Chemical effects of total emissions

Since two reaction rates are relatively quick in atmospheric chemistry, the chemical system tends to obtain chemical equilibrium in the daytime. We use the model outputs of total emission to analyze chemical effects. Using the NO_2/NO_x ratio can judge whether the photodissociation is leading or the reaction of NO and O_3 is leading in the chemical system. The analyses in Fig. 15 & 16 focus on a single point in plain and mountain regions, respectively following the same method of investigating physical effects. In Fig. 15, vehicle pollution is emitted after 6:30 over the plain region. NO reacts to initial O_3 due to

doi:10.6342/NTU202201146

the high emitted NO/NO_2 ratio, while the photodissociation also starts after sunrise. These two effects compete, resulting in a decrease in O_3 and an increase in NO and NO_2. After 8:00, the boundary layer starts to develop. The growth of boundary layer height induces vertical mixing; therefore, NO and NO_2 decrease, and O_3 increases. However, NO_2/NO_x ratio doesn't change a lot during this period, chemical system roughly reaches chemical equilibrium. At 16:00, industrial emissions with a high NO/NO_2 ratio are transported into inland regions by the sea breeze, which caused the NO_2/NO_x ratio slightly dropped, resulting in a decrease in O_3 and an increase in NO and NO_2. Besides, the photolysis rate *j* declines in the afternoon because solar radiation decreases, then the photodissociation stops at 17:30. At night, all NO reacts to background O_3, and NO_2/NO_x ratio rises to 1. On day 2 afternoon, excessive NO is transported by the sea breeze. A lower NO_2/NO_x ratio can be observed in the plain region. Under an unfavorable meteorological condition for pollution dispersion, O_3 runs out at 17:00, which also inhibits NO_2 production and changes the proportion of NO and NO_2 at night. On the other hand, chemical effects in the mountain region are relatively simple, showed in Fig. 16. Photodissociation dominated in the daytime, resulting in a decrease in NO_2 and an increase in NO and O_3 with the NO_2/NO_x ratio drops. At night, NO reacts to background O_3 to produce NO_2, and NO_2/NO_x ratio rises to 1. Besides, the lack of O_3 also happens on day 2 at 18:30 in the mountain region.

doi:10.6342/NTU202201146

Since the chemical system in our idealized simulation is based on the atmospheric cycle of nitrogen dioxide, nitric oxide, and ozone, the system is expected to be in a photochemical steady state. It is able to determine a photochemical steady-state through the Leighton relationship (Leighton, 1961; Ridley et al., 1992):

$$Leighton\ ratio\ \Phi = \frac{j \cdot NO_2}{k \cdot NO \cdot O_3} \quad (4)$$

when Φ = 1, the system reaches a photochemical steady state because of quick chemical reactions. The time evolution of the Leighton ratio in different regions is shown in Fig. 17. The ratios mostly hold at 0.9 on day 1 over coastal and inland regions. Lower than 1 might be caused by the high concentration of continuous emissions. The ratios on day 2 are close to 1, which indicates that the chemical condition in most of the land regions has reached a photochemical steady state. In addition, the ratios in mountain regions become extremely high in the early morning, which is influenced by the rapid change in photodissociation rate and concentration of NO.

doi:10.6342/NTU202201146

5 Summary and Discussion

In our study, an idealized simulation of pollution transport in central Taiwan was conducted to investigate the physical and chemical effects involved in pollution transport under weak synoptic weather conditions. Physical effects include local circulation, boundary layer processes, prescribed thermal inversion layer, and chemical products mainly controlled by chemical reactions. Sea breezes control the transport of industrial emissions, and pollution moves with sea breeze worsening air quality, while local maximum drastically decreases from coastal to mountain regions. On the other hand, transport of vehicle emissions is mainly determined by the diurnal evolution of the boundary layer, pollution peak happens in the early morning and is then diluted after the boundary layer develops. Comparing the effects on local air quality between industrial and vehicle emission sources, in the plain region, vehicle pollution has a considerable impact on air quality in the early morning. But industrial pollution can hugely worsen air quality in the coastal region in the whole morning, and air quality in the inland region is affected after the sea breeze arrives. In mountain regions, industrial and vehicle pollution have a similar influence on local air quality. Due to low wind speed and low boundary layer height at night, pollution in the mountain region is difficult to transport and disperse. The concentration of pollution remains for an extended period until the boundary layer develops the next morning. The chemical system shows a diurnal variation depending on

doi:10.6342/NTU202201146

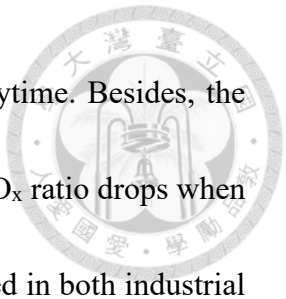

photodissociation, NO_2/NO_x ratio drops, and O_3 produces in the daytime. Besides, the emitted NO/NO_2 ratio also affects chemical equilibrium. The NO_2/NO_x ratio drops when high polluted air is transported into that region, which can be observed in both industrial and vehicle emissions.

Based on our idealized simulations, we have investigated that industrial emission is the critical emission source affecting local air quality in central Taiwan. Industrial emissions worsen air quality in the plain areas during the entire afternoon. Sea breezes also play a crucial role in transporting pollutants. Industrial emissions transported by sea breezes cause pollution events from coastal to mountain regions, and vehicle emissions accumulated by sea breezes worsen air quality over inland regions. Boundary layer processes have been restrained due to the initial profiles. In fact, inversion layer height and surface temperature can vary in the winter leading to different pollution scenarios. For example, a near-surface inversion layer might suppress boundary layer processes, resulting in a prolonged accumulation of vehicle pollution near the surface. In contrast, a higher inversion layer coupled with higher surface temperature is relatively conducive to pollution dispersion, which induces stronger vertical mixing to improve air quality near the surface. We can establish a series of pollution transport structures for the winter in central Taiwan by changing the initial sounding profiles. Analyzing the variation of inversion layer height and surface temperature in the winter can help us construct

doi:10.6342/NTU202201146

simplified composite sounding profiles which cover all the thermal information in wintertime. By using these sounding profiles, we can conduct a series of idealized simulations to specify the variation of physical and chemical effects on pollution transport. Once we understand the variation of physical effects on pollution transport, it is able to control emission sources and reduce air pollution events by verifying corresponding meteorological conditions. On the other hand, a more complex chemical system can help us get closer to the actual observation and directly quantify the impact of pollutants on local air quality. We might be able to consider a chemical system that covers more critical reactions affecting NO_x pollution, such as reactions of Volatile Organic Compounds (VOCs) and nocturnal NO_3 radical chemistry.

doi:10.6342/NTU202201146

References

Arakawa, A., & Wu, C.-M. (2013, 01 Jul. 2013). A Unified Representation of Deep Moist Convection in Numerical Modeling of the Atmosphere. Part I. *Journal of the Atmospheric Sciences, 70*(7), 1977-1992. https://doi.org/https://doi.org/10.1175/jas-d-12-0330.1

Brown, A. R., Cederwall, R. T., Chlond, A., Duynkerke, P. G., Golaz, J.-C., Khairoutdinov, M., Lewellen, D. C., Lock, A. P., MacVean, M. K., Moeng, C.-H., Neggers, R. A. J., Siebesma, A. P., & Stevens, B. (2002). Large-eddy simulation of the diurnal cycle of shallow cumulus convection over land. *Quarterly Journal of the Royal Meteorological Society, 128*(582), 1075-1093. https://doi.org/https://doi.org/10.1256/003590002320373210

Chang, Y. H., Chen, W. T., Wu, C. M., Moseley, C., & Wu, C. C. (2021). Tracking the influence of cloud condensation nuclei on summer diurnal precipitating systems over complex topography in Taiwan. *Atmos. Chem. Phys., 21*(22), 16709-16725. https://doi.org/https://doi.org/10.5194/acp-21-16709-2021

Chen, F., & Dudhia, J. (2001, 01 Apr. 2001). Coupling an Advanced Land Surface–Hydrology Model with the Penn State–NCAR MM5 Modeling System. Part I: Model Implementation and Sensitivity. *Monthly Weather Review, 129*(4), 569-585. https://doi.org/https://doi.org/10.1175/1520-0493(2001)129<0569:Caalsh>2.0.Co;2

Chen, F., Mitchell, K., Schaake, J., Xue, Y., Pan, H.-L., Koren, V., Duan, Q. Y., Ek, M., & Betts, A. (1996). Modeling of land surface evaporation by four schemes and comparison with FIFE observations. *Journal of Geophysical Research: Atmospheres, 101*(D3), 7251-7268. https://doi.org/https://doi.org/10.1029/95JD02165

Chen, W.-T., Wu, C.-M., Tsai, W.-M., Chen, P.-J., & Chen, P.-Y. (2019). Role of Coastal Convection to Moisture Buildup during the South China Sea Summer Monsoon Onset. *Journal of the Meteorological Society of Japan. Ser. II, 97*(6), 1155-1171. https://doi.org/https://doi.org/10.2151/jmsj.2019-065

Cheng, W.-L. (2001, 2001/10/01/). Synoptic weather patterns and their relationship to high ozone concentrations in the Taichung Basin. *Atmospheric Environment,*

doi:10.6342/NTU202201146

35(29), 4971-4994. https://doi.org/https://doi.org/10.1016/S1352-2310(01)00295-3

Cheng, W.-L. (2002). Ozone distribution in coastal central Taiwan under sea-breeze conditions. *Atmospheric Environment, 36*(21), 3445-3459. https://doi.org/https://doi.org/10.1016/S1352-2310(02)00307-2

Cheng, W.-L., Pai, J.-L., Tsuang, B.-J., & Chen, C.-L. (2001). Synoptic patterns in relation to ozone concentrations in west-central Taiwan. *Meteorology and Atmospheric Physics, 78*(1), 11-21. https://doi.org/https://doi.org/10.1007/s007030170002

Chien, M.-H., & Wu, C.-M. (2016). Representation of topography by partial steps using the immersed boundary method in a vector vorticity equation model (VVM). *Journal of Advances in Modeling Earth Systems, 8*(1), 212-223. https://doi.org/https://doi.org/10.1002/2015MS000514

Chiu, H.-F., Weng, Y.-H., Chiu, Y.-W., & Yang, C.-Y. (2015). Air pollution and daily clinic visits for headache in a subtropical city: Taipei, Taiwan. *International Journal of Environmental Research and Public Health, 12*(2), 2277-2288. https://doi.org/https://doi.org/10.3390/ijerph120202277

Garratt, J. R. (1994). The atmospheric boundary layer. *Earth-Science Reviews, 37*(1-2), 89-134. https://doi.org/https://doi.org/10.1016/0012-8252(94)90026-4

Heus, T., van Heerwaarden, C. C., Jonker, H. J. J., Pier Siebesma, A., Axelsen, S., van den Dries, K., Geoffroy, O., Moene, A. F., Pino, D., de Roode, S. R., & Vilà-Guerau de Arellano, J. (2010). Formulation of the Dutch Atmospheric Large-Eddy Simulation (DALES) and overview of its applications. *Geosci. Model Dev., 3*(2), 415-444. https://doi.org/https://doi.org/10.5194/gmd-3-415-2010

Hsieh, M.-K., Chen, Y.-W., Chen, Y.-C., & Wu, C.-M. (2022, 01/01). The Roles of Local Circulation and Boundary Layer Development in Tracer Transport over Complex Topography in Central Taiwan. *Journal of the Meteorological Society of Japan. Ser. II*. https://doi.org/https://doi.org/10.2151/jmsj.2022-028

Hsu, C.-H., & Cheng, F.-Y. (2019). Synoptic Weather Patterns and Associated Air Pollution in Taiwan. *Aerosol and Air Quality Research, 19*(5), 1139-1151. https://doi.org/https://doi.org/10.4209/aaqr.2018.09.0348

doi:10.6342/NTU202201146

Hsu, T.-H. (2021). *The Fine Particulate Pollutants Distribution over the Lee Side of Mountains in Taiwan under Consecutive Cold-season Weak Synoptic Days* [Master Thesis, National Taiwan University]. http://dx.doi.org/10.6342/NTU202101073

Huang, J.-D., & Wu, C.-M. (2022). A Framework to Evaluate Convective Aggregation: Examples With Different Microphysics Schemes. *Journal of Geophysical Research: Atmospheres, 127*(5), e2021JD035886. https://doi.org/https://doi.org/10.1029/2021JD035886

Jung, C.-R., Chen, W.-T., Tang, Y.-H., & Hwang, B.-F. (2019, 2019/06/01/). Fine particulate matter exposure during pregnancy and infancy and incident asthma. *Journal of Allergy and Clinical Immunology, 143*(6), 2254-2262.e2255. https://doi.org/https://doi.org/10.1016/j.jaci.2019.03.024

Jung, J.-H., & Arakawa, A. (2008). A Three-Dimensional Anelastic Model Based on the Vorticity Equation. *Monthly Weather Review, 136*, 276-294. https://doi.org/https://doi.org/10.1175/2007MWR2095.1

Kuo, K.-T., & Wu, C.-M. (2019). The Precipitation Hotspots of Afternoon Thunderstorms over the Taipei Basin: Idealized Numerical Simulations. *Journal of the Meteorological Society of Japan. Ser. II, 97*(2), 501-517. https://doi.org/https://doi.org/10.2151/jmsj.2019-031

Kuo, P.-H., Tsuang, B.-J., Chen, C.-J., Hu, S.-W., Chiang, C.-J., Tsai, J.-L., Tang, M.-L., Chen, G.-J., & Ku, K.-C. (2014, 2014/10/01/). Risk assessment of mortality for all-cause, ischemic heart disease, cardiopulmonary disease, and lung cancer due to the operation of the world's largest coal-fired power plant. *Atmospheric Environment, 96*, 117-124. https://doi.org/https://doi.org/10.1016/j.atmosenv.2014.07.024

Leighton, P. (1961). *Photochemistry of air pollution*. Elsevier.

Liang, W.-M., Wei, H.-Y., & Kuo, H.-W. (2009). Association between daily mortality from respiratory and cardiovascular diseases and air pollution in Taiwan. *Environmental research, 109*(1), 51-58. https://doi.org/https://doi.org/10.1016/j.envres.2008.10.002

doi:10.6342/NTU202201146

Ma, J.-W., Lai, T.-J., Hu, S.-Y., Lin, T.-C., Ho, W.-C., & Tsan, Y.-T. (2020). Effect of ambient air pollution on the incidence of colorectal cancer among a diabetic population: a nationwide nested case–control study in Taiwan. *BMJ open, 10*(10), e036955. https://doi.org/https://doi.org/10.1136/bmjopen-2020-036955

Ridley, B., Madronich, S., Chatfield, R., Walega, J., Shetter, R., Carroll, M., & Montzka, D. (1992). Measurements and model simulations of the photostationary state during the Mauna Loa Observatory Photochemistry Experiment: Implications for radical concentrations and ozone production and loss rates. *Journal of Geophysical Research: Atmospheres, 97*(D10), 10375-10388. https://doi.org/https://doi.org/10.1029/91JD02287

Su, S.-H., Chang, C.-W., & Chen, W.-T. (2020). The Temporal Evolution of PM2.5 Pollution Events in Taiwan: Clustering and the Association with Synoptic Weather. *Atmosphere, 11*(11), 1265. https://doi.org/https://doi.org/10.3390/atmos11111265

Tsai, D.-H., Wang, J.-L., Chuang, K.-J., & Chan, C.-C. (2010). Traffic-related air pollution and cardiovascular mortality in central Taiwan. *Science of the total environment, 408*(8), 1818-1823. https://doi.org/https://doi.org/10.1016/j.scitotenv.2010.01.044

Tsai, J.-Y., & Wu, C.-M. (2016, 2016/12/01/). Critical transitions of stratocumulus dynamical systems due to perturbation in free-atmosphere moisture. *Dynamics of Atmospheres and Oceans, 76*, 1-13. https://doi.org/https://doi.org/10.1016/j.dynatmoce.2016.08.002

Tsai, W.-M., & Wu, C.-M. (2017). The environment of aggregated deep convection. *Journal of Advances in Modeling Earth Systems, 9*(5), 2061-2078. https://doi.org/https://doi.org/10.1002/2017MS000967

Tseng, C.-H., Tsuang, B.-J., Chiang, C.-J., Ku, K.-C., Tseng, J.-S., Yang, T.-Y., Hsu, K.-H., Chen, K.-C., Yu, S.-L., & Lee, W.-C. (2019). The relationship between air pollution and lung cancer in nonsmokers in Taiwan. *Journal of Thoracic Oncology, 14*(5), 784-792. https://doi.org/https://doi.org/10.1016/j.jtho.2018.12.033

Verwer, J. G. (1994). Gauss-Seidel Iteration for Stiff ODES from Chemical Kinetics. *SIAM J. Sci. Comput., 15*, 1243-1250.

doi:10.6342/NTU202201146

https://doi.org/https://doi.org/10.1137/0915076

Verwer, J. G., & Simpson, D. (1995, 1995/09/01/). Explicit methods for stiff ODEs from atmospheric chemistry. *Applied Numerical Mathematics, 18*(1), 413-430. https://doi.org/https://doi.org/10.1016/0168-9274(95)00068-6

Vilà-Guerau de Arellano, J., Kim, S. W., Barth, M. C., & Patton, E. G. (2005). Transport and chemical transformations influenced by shallow cumulus over land. *Atmos. Chem. Phys., 5*(12), 3219-3231. https://doi.org/https://doi.org/10.5194/acp-5-3219-2005

Vilà-Guerau de Arellano, J., van den Dries, K., & Pino, D. (2009). On inferring isoprene emission surface flux from atmospheric boundary layer concentration measurements. *Atmos. Chem. Phys., 9*(11), 3629-3640. https://doi.org/https://doi.org/10.5194/acp-9-3629-2009

Wu, C.-M., & Arakawa, A. (2011, 06/21). Inclusion of Surface Topography into the Vector Vorticity Equation Model (VVM). *Journal of Advances in Modeling Earth Systems, 3*. https://doi.org/https://doi.org/10.1029/2011MS000061

Wu, C.-M., & Arakawa, A. (2014, 01 Jun. 2014). A Unified Representation of Deep Moist Convection in Numerical Modeling of the Atmosphere. Part II. *Journal of the Atmospheric Sciences, 71*(6), 2089-2103. https://doi.org/https://doi.org/10.1175/jas-d-13-0382.1

Wu, C.-M., & Chen, P.-Y. (2021). Idealized cloud-resolving simulations of land-atmosphere coupling over tropical islands. *Terrestrial, Atmospheric & Oceanic Sciences, 32*(2). https://doi.org/https://doi.org/10.3319/TAO.2020.12.16.01

Wu, C.-M., Lin, H.-C., Cheng, F.-Y., & Chien, M.-H. (2019, 04/08). Implementation of the Land Surface Processes into a Vector Vorticity Equation Model (VVM) to Study its Impact on Afternoon Thunderstorms over Complex Topography in Taiwan. *Asia-Pacific Journal of Atmospheric Sciences, 55*. https://doi.org/https://doi.org/10.1007/s13143-019-00116-x

Wu, C.-M., Lo, M.-H., Chen, W.-T., & Lu, C.-T. (2015). The impacts of heterogeneous land surface fluxes on the diurnal cycle precipitation: A framework for improving the GCM representation of land-atmosphere interactions. *Journal of Geophysical*

doi:10.6342/NTU202201146

Research: Atmospheres, 120(9), 3714-3727. https://doi.org/https://doi.org/10.1002/2014JD023030

Yu, T.-Y., & Chang, I.-C. (2006). Spatiotemporal Features of Severe Air Pollution in Northern Taiwan (8 pp). *Environmental Science and Pollution Research, 13*(4), 268-275. https://doi.org/https://doi.org/10.1065/espr2005.12.288

doi:10.6342/NTU202201146

Tables

Table 1: The surface fluxes of chemical species prescribed in the comparison test.

	surface fluxes
inert tracer	0.1 ppb·m/s
NO	0.1 ppb·m/s
NO_2	0.05 ppb·m/s
O_3	0.0 ppb·m/s

doi:10.6342/NTU202201146

Table 2: The emission setting of industrial and vehicle emission sources. Industrial emission represents the pollution from power and steel industries in coastal industrial parks, and the emission height is set at 300m which refers to the stack height of power plants. Vehicle emission in urban areas is mainly associated with human activities; therefore, the pollution duration is set in the daytime. We use Taiwan emission database system version 11.0 (TEDS 11.0) based on 2019 in Taichung as our dataset.

	Industrial emission	Vehicle emission
Region	coastal areas	urban areas
Grid points	1 x 64	254 x 64
Height	300m	surface
Emission time	24 hours	Daytime(6:30-17:20)
NO_x emission	1.899 ppb/(s·grid)	0.01924 ppb/(s·grid)

doi:10.6342/NTU202201146

Figures

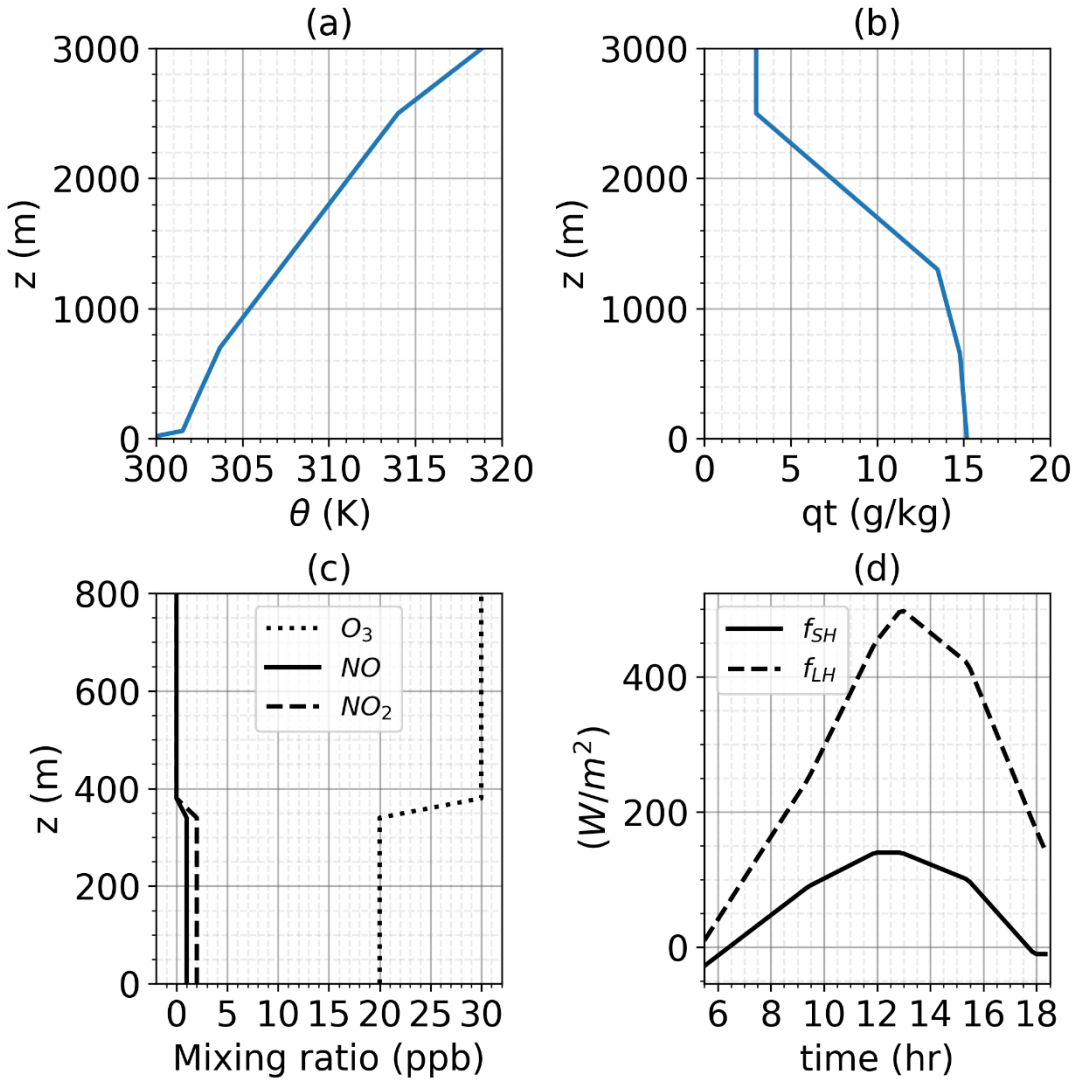

Fig. 1: Initial profiles of (a) potential temperature, (b) total water mixing ratio, (c) chemical species, and (d) the diurnal evolution of sensible and latent heat fluxes.

doi:10.6342/NTU202201146

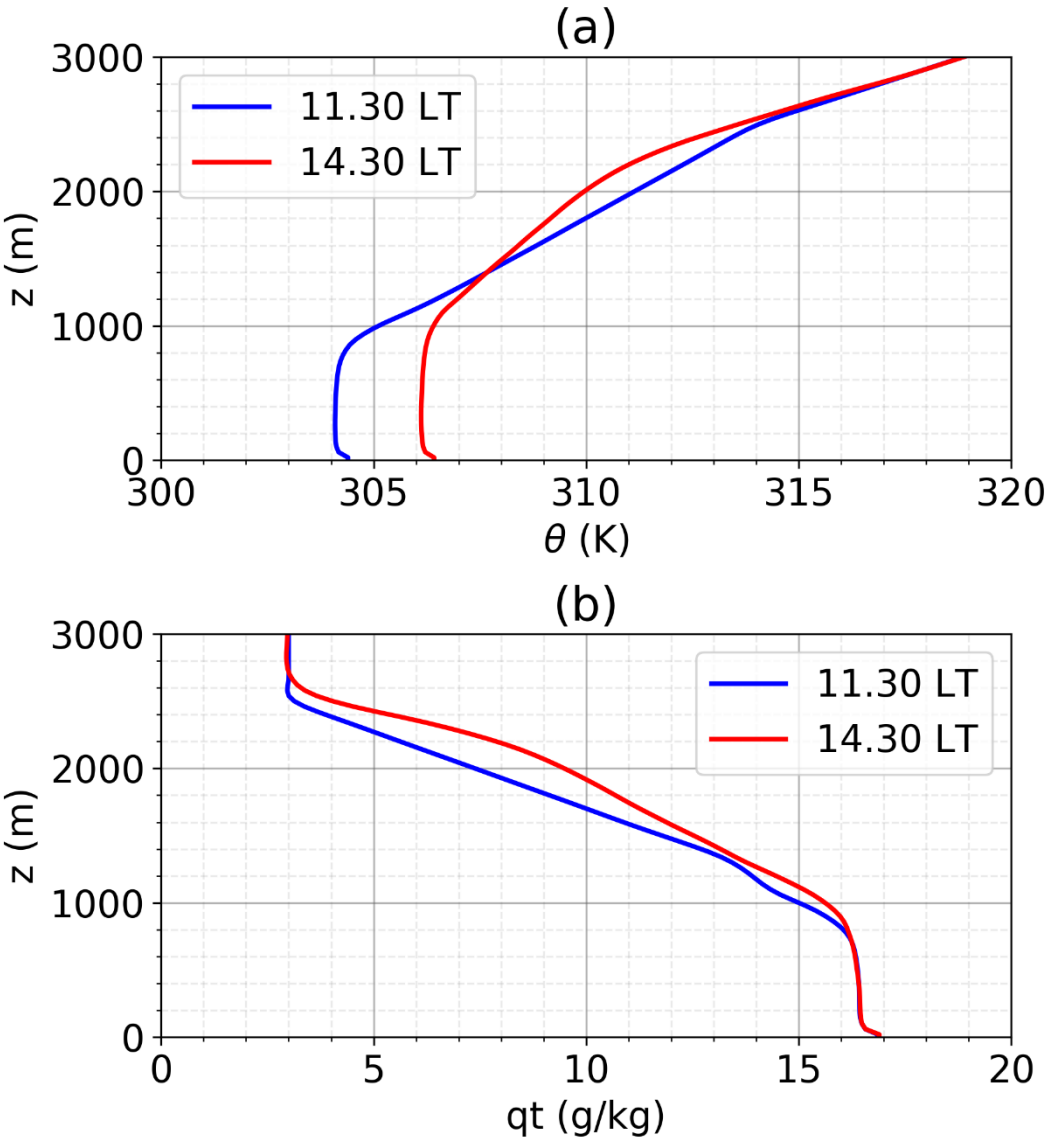

Fig. 2: One-hour averaged vertical profiles of (a) potential temperature and (b) total water mixing ratio at 11:30 LT (blue) and 14:30 LT (red).

doi:10.6342/NTU202201146

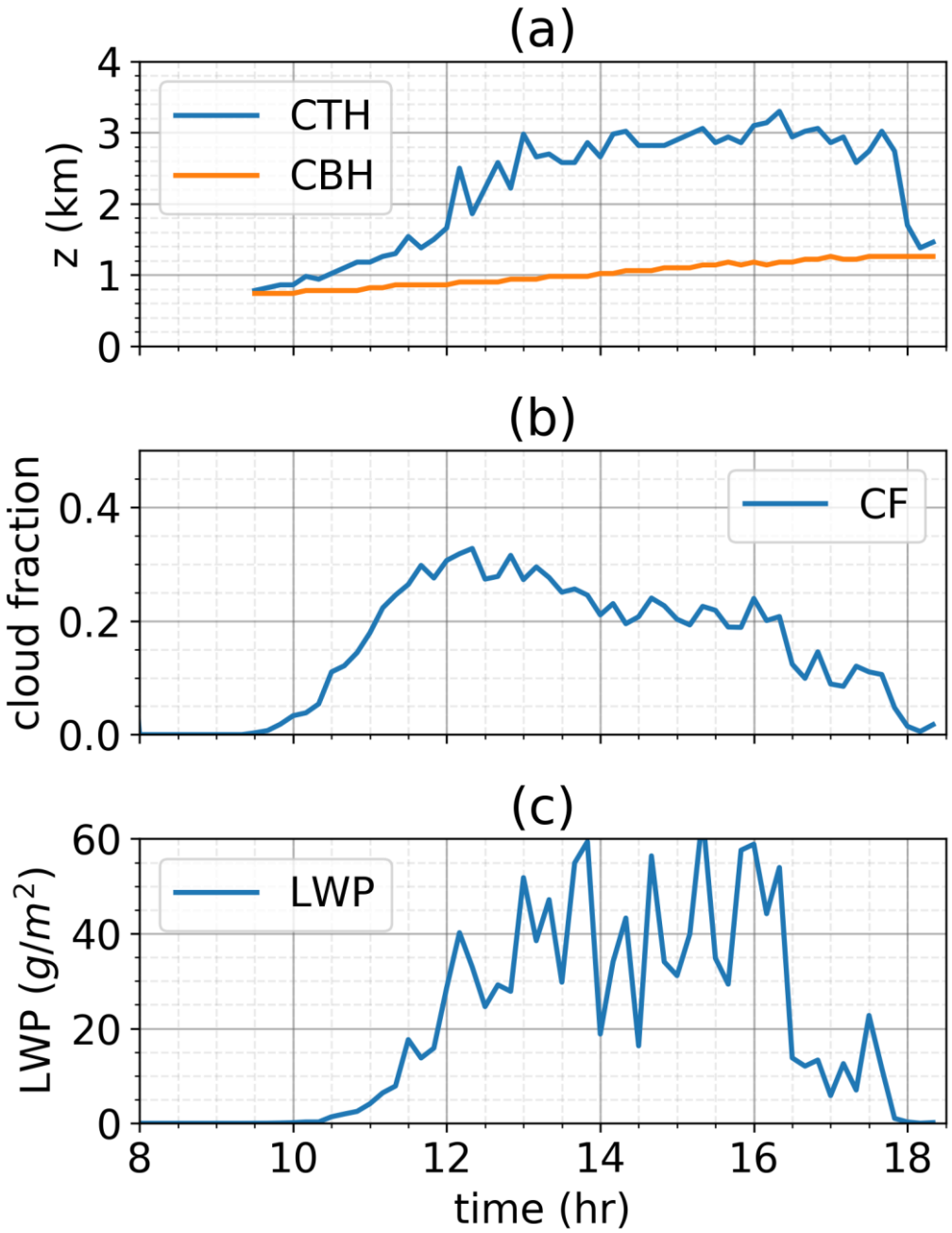

Fig. 3: Time evolution of (a) cloud top height (CTH) and cloud base height (CBH), (b) cloud fraction, and (c) liquid water path.

doi:10.6342/NTU202201146

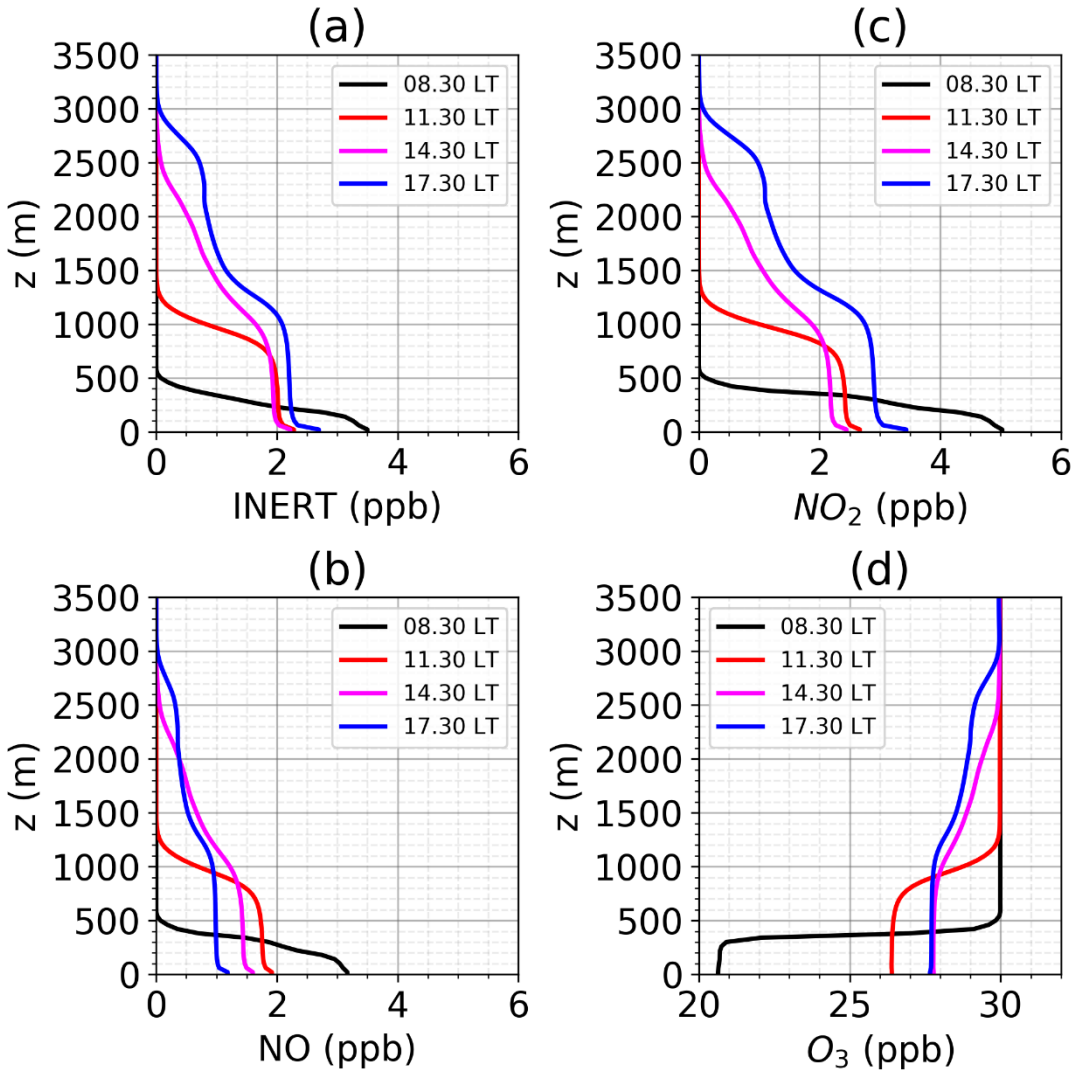

Fig. 4: One-hour slab averaged vertical profiles of (a) inert scalar, (b) NO, (c) NO_2, and (d) O_3 at 8:30 LT (black), 11:30 LT (red), 14:30 LT (pink) and 17:30 LT (blue).

doi:10.6342/NTU202201146

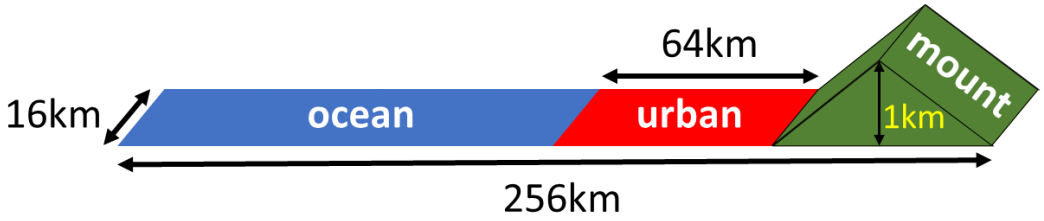

Fig. 5: The ocean, land, and mountain arrangement in the idealized simulation represents the simplification of the terrain of central Taiwan. The setting of half ocean and half land is able to favor the formation of land-sea breeze. Since Noah LSM version 3.4.1 is implemented to VVM (Wu et al., 2019), different land use can be separated and specified in the idealized simulation, thus the land is separated into urban areas (red, LU=1) and mountain areas (green, LU=13) to imitate Taichung downtown areas and the Central Mountain Range. The mountain areas are bilateral symmetry on the x-axis and the mountain height is set at 1000m, the real height of the Central Mountain Range is not applied in the simulation to avoid computing issues.

doi:10.6342/NTU202201146

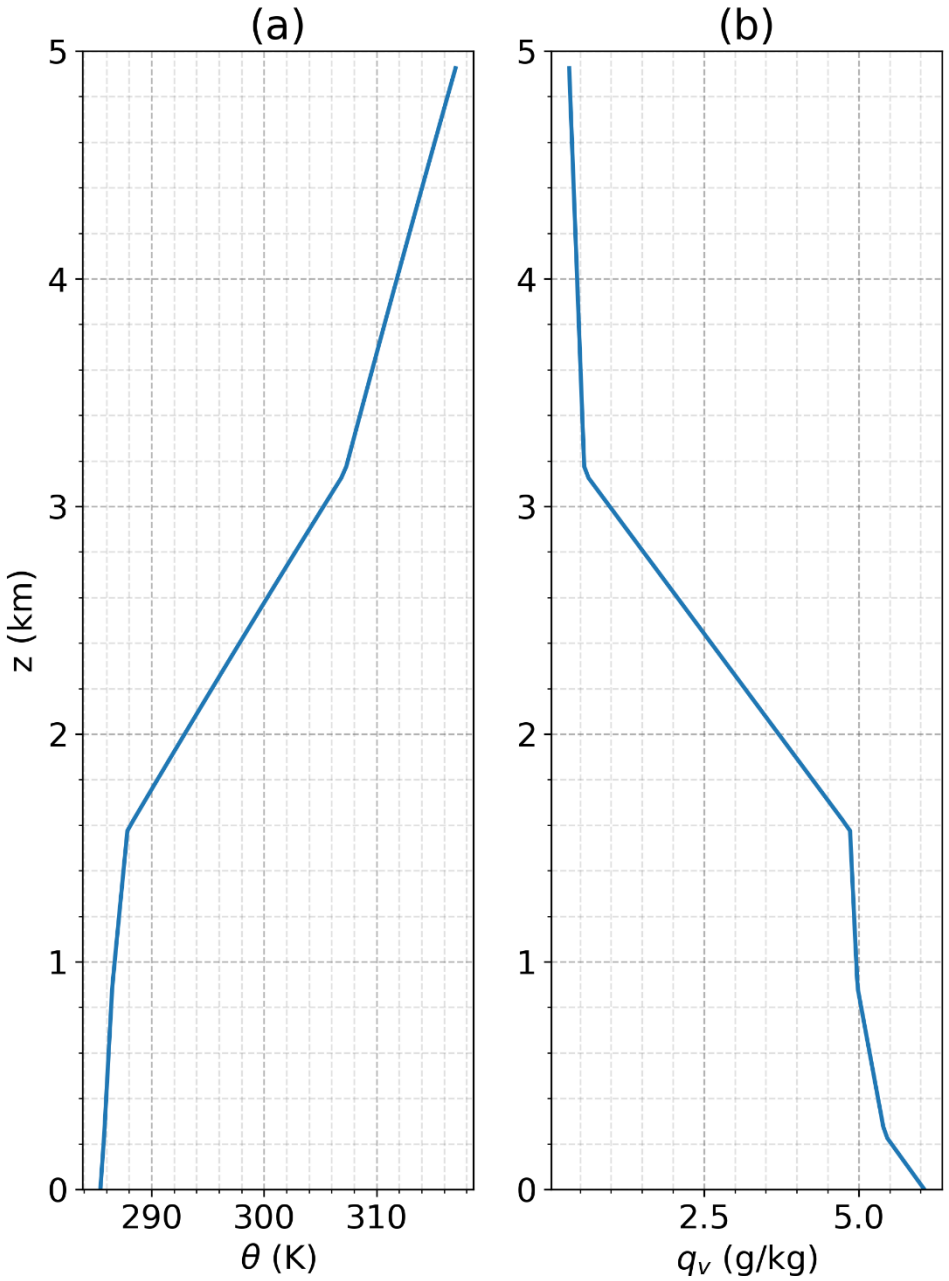

Fig. 6: The initial profiles of (a) potential temperature and (b) water vapor mixing ratio which represents idealized winter condition in Taiwan. A thermal inversion layer can be observed from 1600m to 3200m.

doi:10.6342/NTU202201146

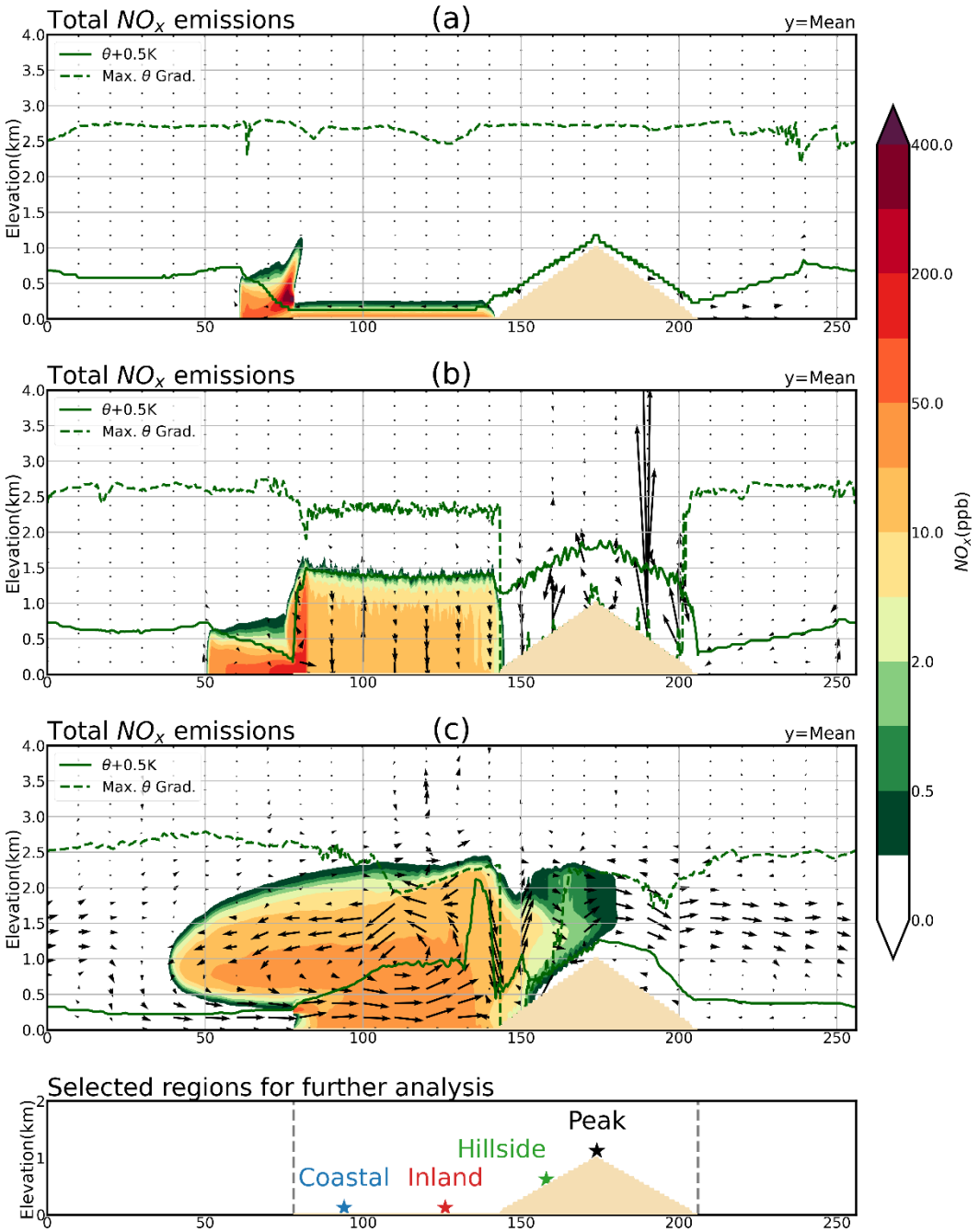

Fig. 7: Y-axis mean cross-section vertical profiles of NO_x concentration on day 1 (a) 07:30 LT, (b) 10:30 LT, and (c) 16:30 LT are shown in the upper figure. Quivers represent wind profiles in the x-z plane. Green solid lines represent the boundary layer height defined by surface potential temperature + 0.5K, and green dashed lines represent the boundary layer height defined by the maximum gradient of potential temperature under 3000m. Selected regions for further analysis (Fig. 8-17) are shown in the lower figure.

doi:10.6342/NTU202201146

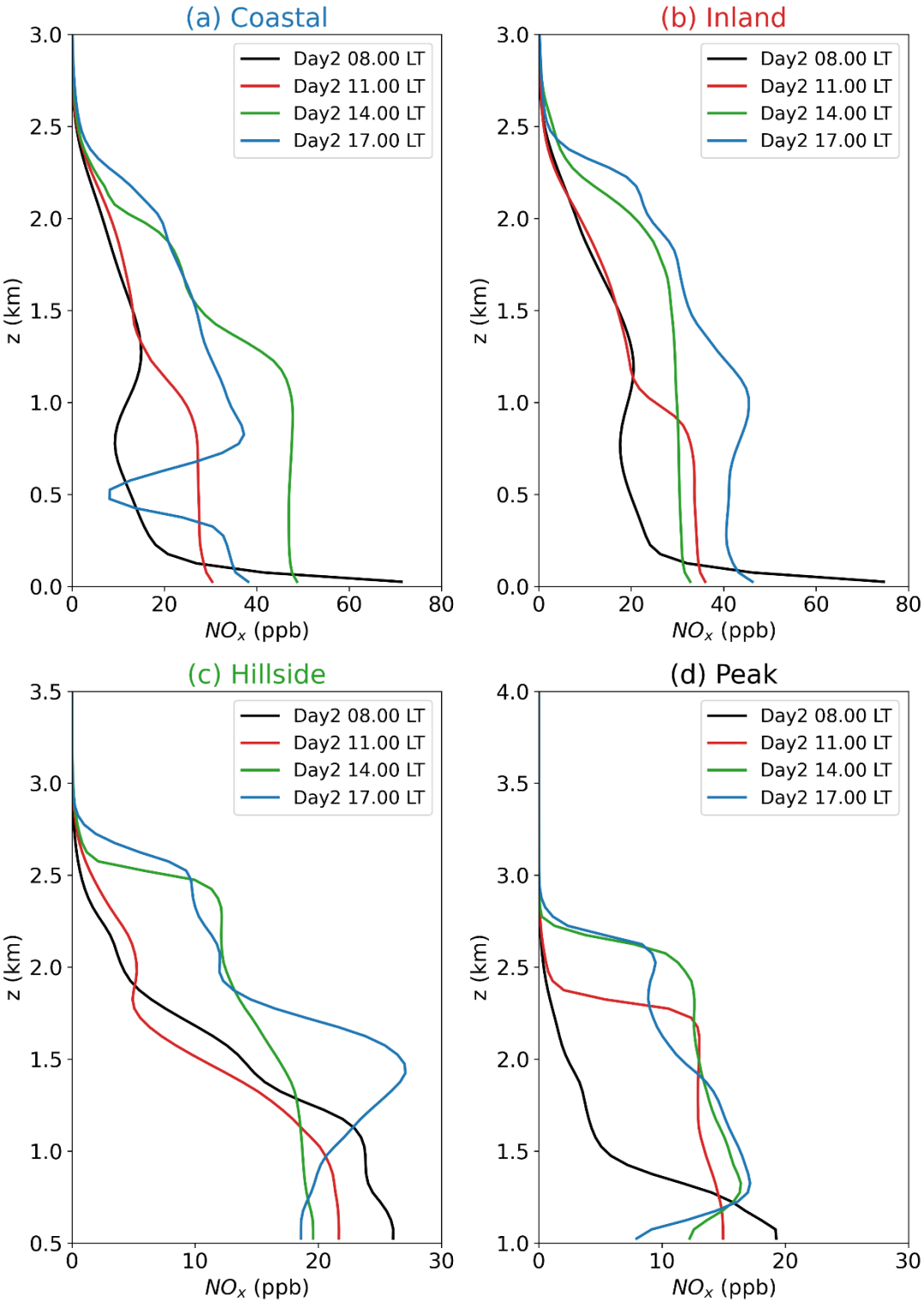

Fig. 8: Vertical profiles of NO_x concentration over (a) coastal, (b) inland, (c) hillside, and (d) peak regions on day 2 8:00 LT (black), 11:00 LT (red), 14:00 LT (green), and 17:00 LT (blue).

doi:10.6342/NTU202201146

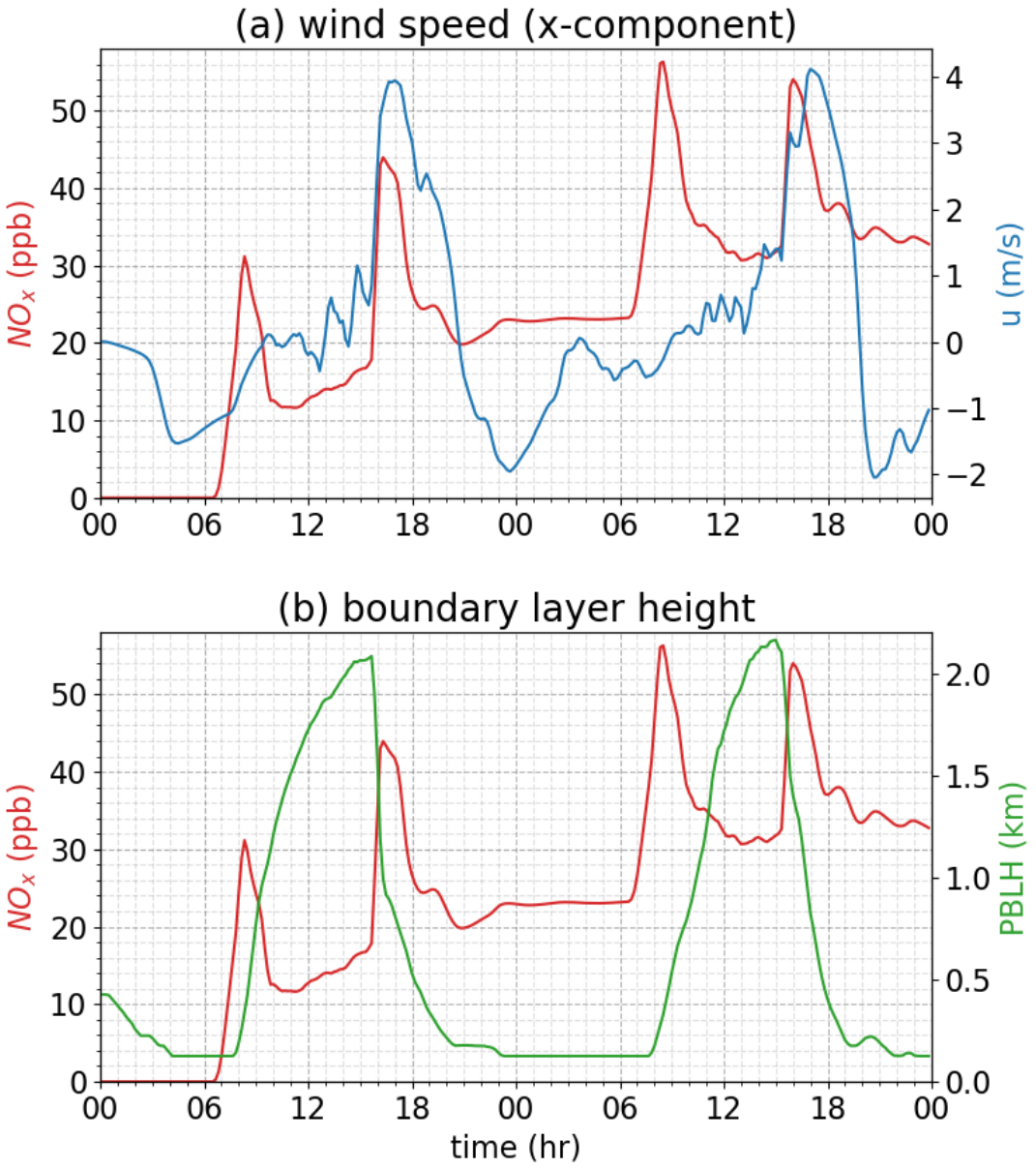

Fig. 9: Time evolution of (a) sea breeze strength (blue), (b) boundary layer height (green), and NO_x concentration (red) over the inland region.

doi:10.6342/NTU202201146

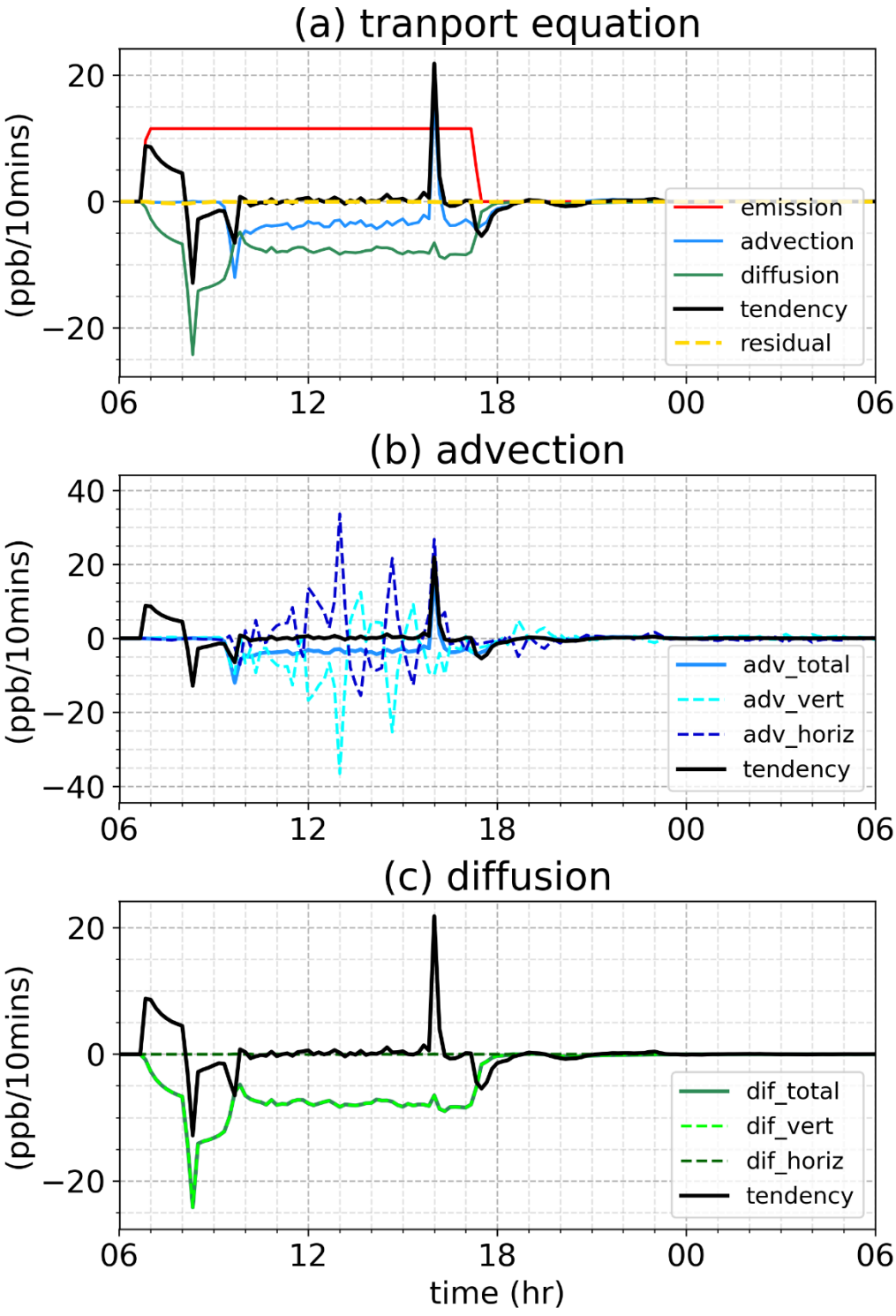

Fig. 10: Time evolution of the budget of (a) transport equation, (b) advection terms, and (c) diffusion terms over the inland region. Total budgets include tendency (black), emission (red), advection (blue), diffusion (green), and residual terms (yellow dashed). Advection and diffusion in (b) and (c) are separated into horizontal (dark color) and vertical (light color) terms shown in dashed lines.

doi:10.6342/NTU202201146

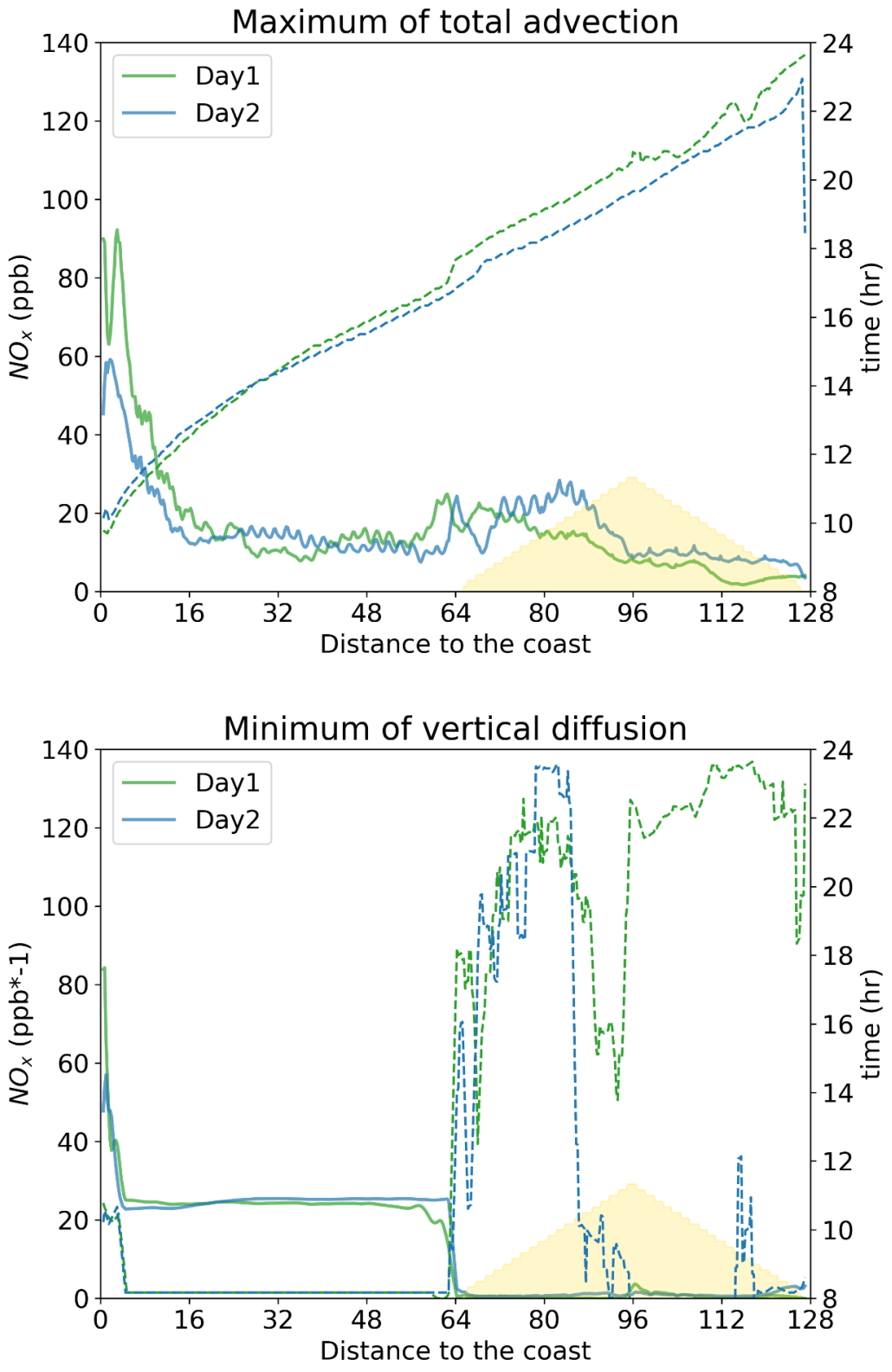

Fig. 11: Extreme values and the peak times of total advection and vertical diffusion over land regions on day 1 (green) and day 2 (blue), respectively. Solid lines show the peak values and dashed lines show the peak times. Minimums of vertical diffusion are multiplied by -1 to compare to the maximum of total advection easily.

doi:10.6342/NTU202201146

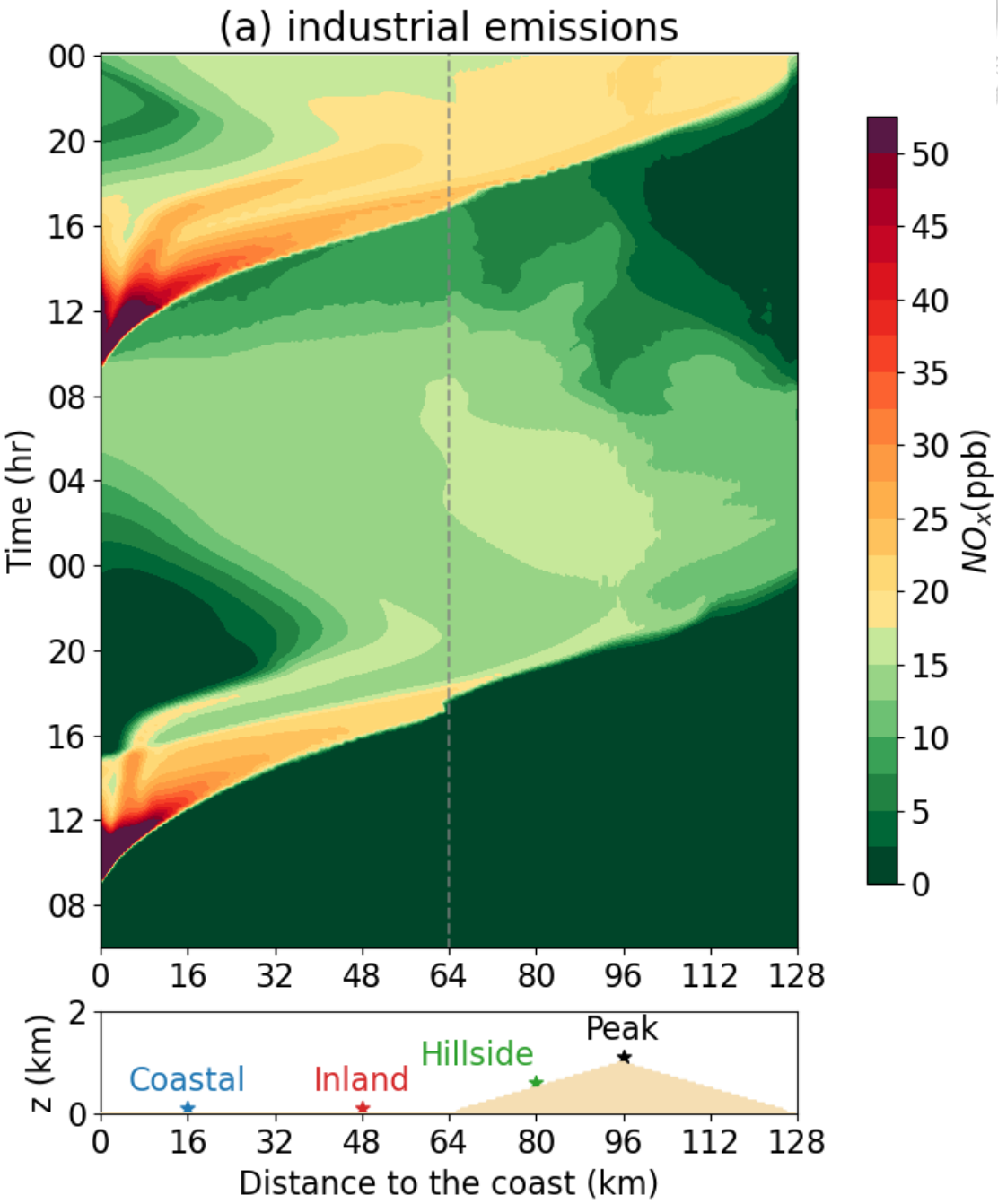

Fig. 12(a): The time series of surface NO_x concentration of industrial emissions over land regions only. Shaded represents NO_x concentration. Gray dashed lines represent the boundary between plains and mountains.

doi:10.6342/NTU202201146

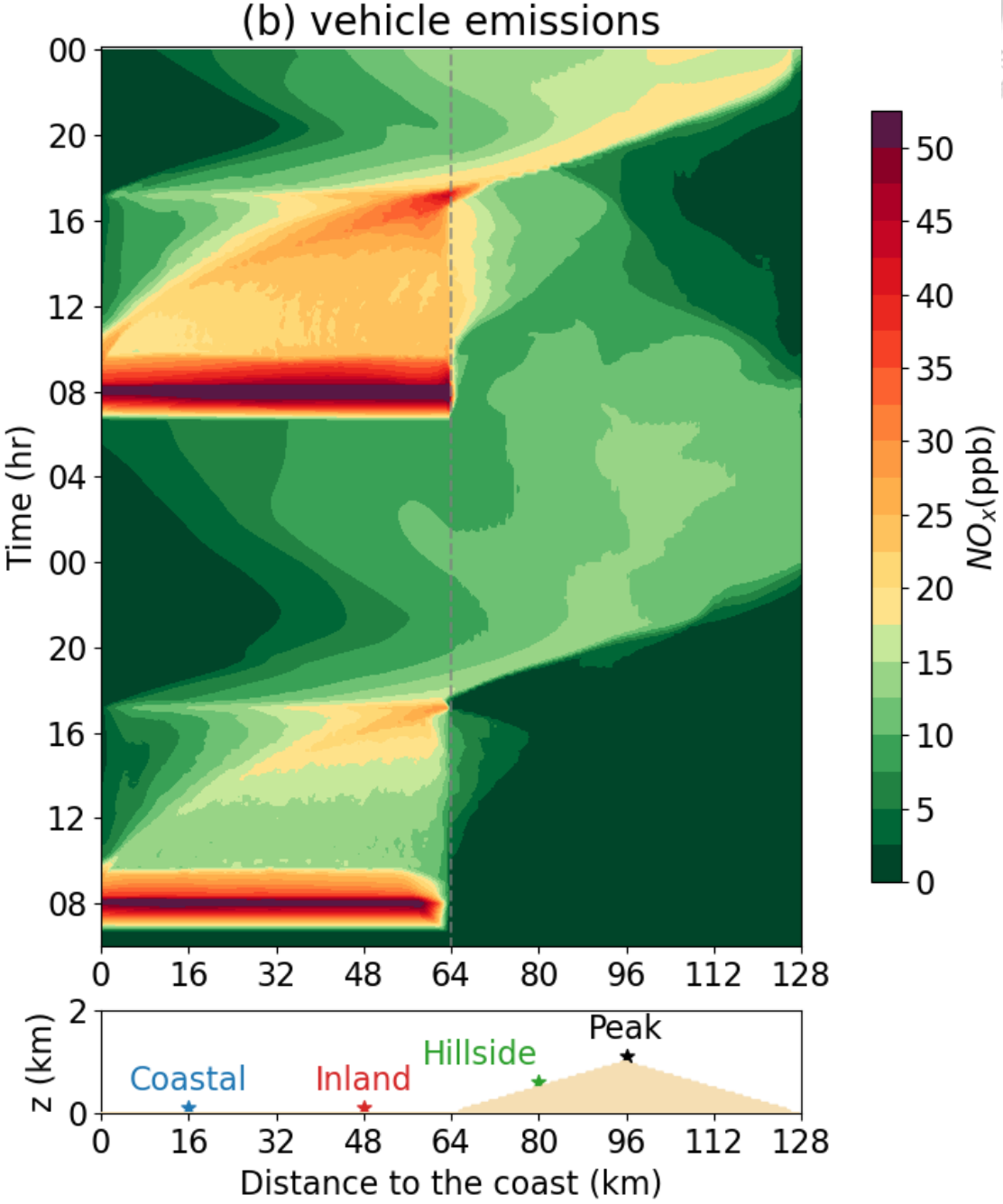

Fig. 12(b): The time series of surface NO_x concentration of vehicle emissions over land regions only. Shaded represents NO_x concentration. Gray dashed lines represent the boundary between plains and mountains.

doi:10.6342/NTU202201146

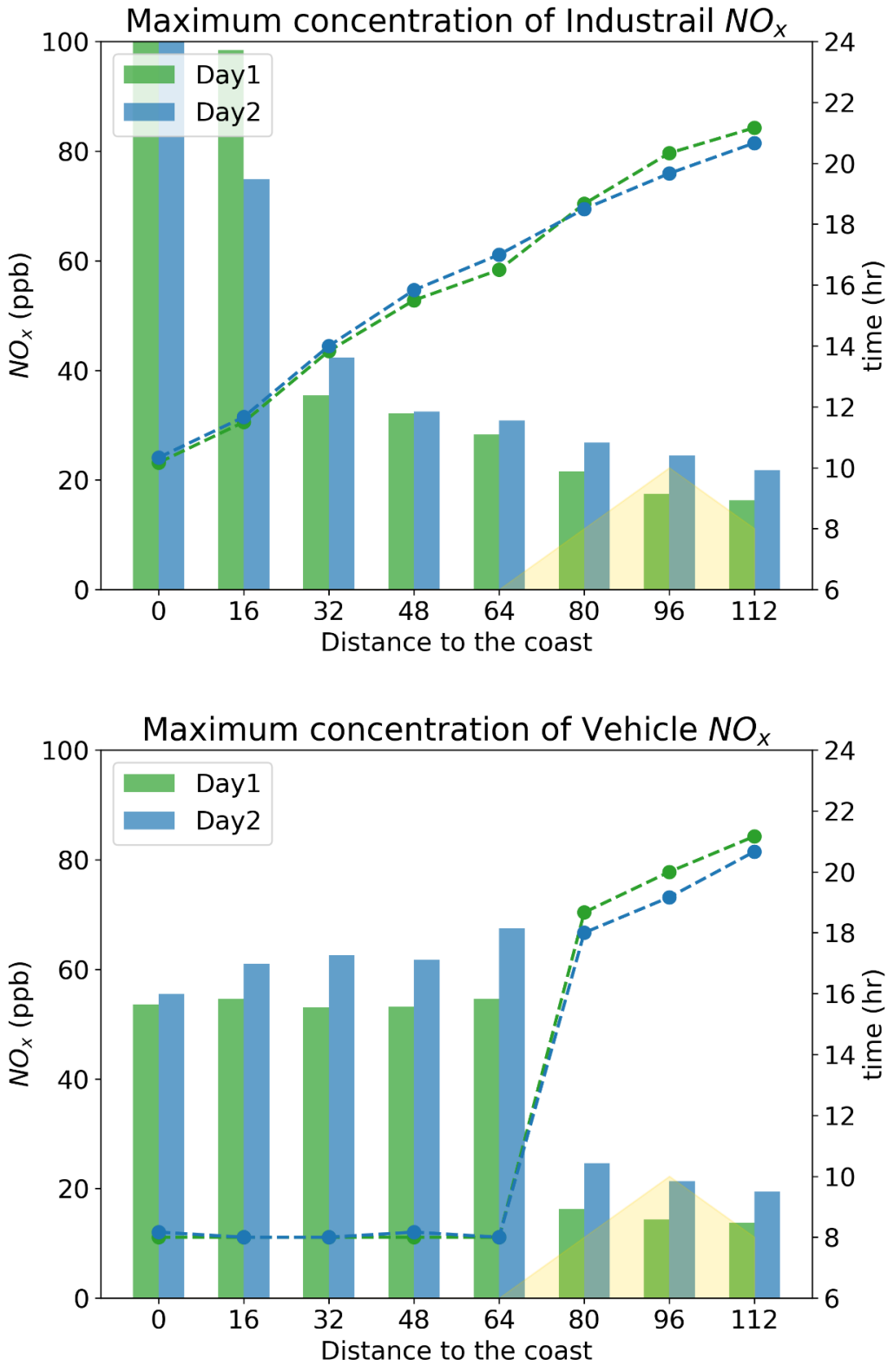

Fig. 13: Maximum concentrations and the peak times of industrial and vehicle emission over land regions on day 1 (green) and day 2 (blue), respectively. Bar charts show the peak values and dashed lines show the peak times. Land regions were divided into eight areas to be analyzed.

doi:10.6342/NTU202201146

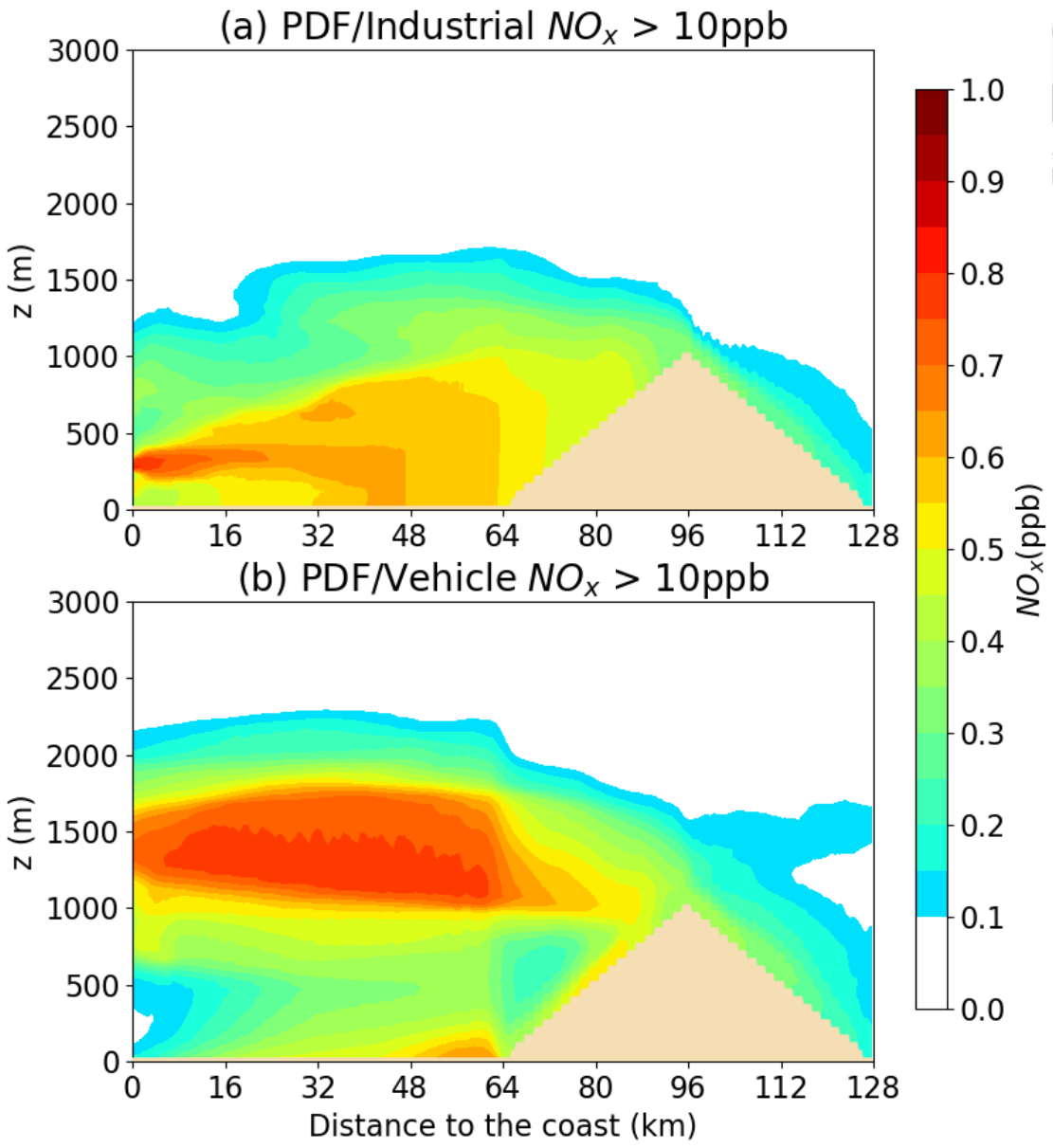

Fig. 14: Probability Density Function of the occurrence of the concentration of (a) industrial and (b) vehicle NO_x larger than 10 ppb in the x-z plane. The larger the shaded is shown, the longer the NO_x concentration larger than 10 ppb would stay in there. The probability of 1 represents that NO_x concentration is larger than 10 ppb for up to two days.

doi:10.6342/NTU202201146

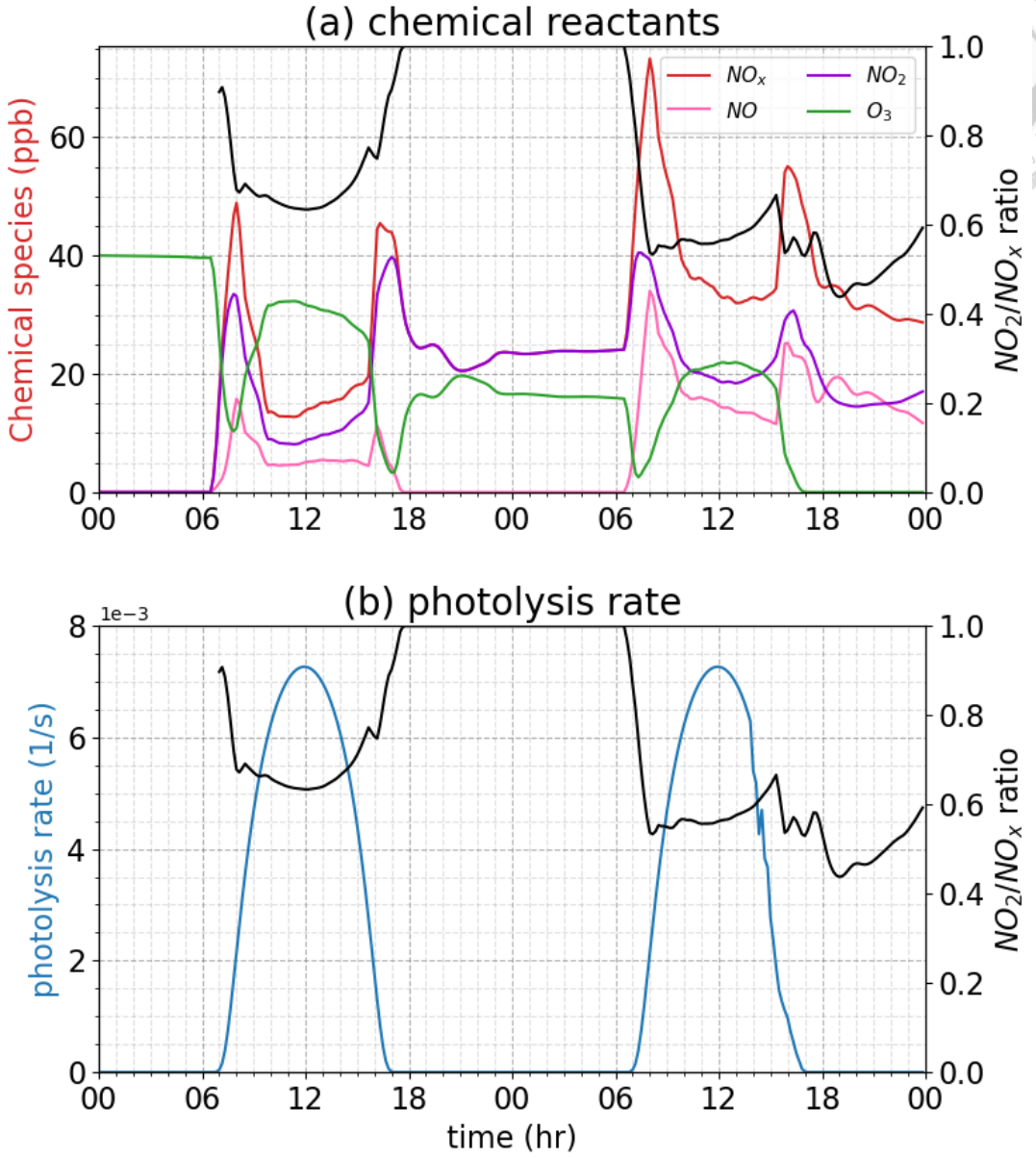

Fig. 15: Time evolution of (a) NO_x (red), NO (pink), NO_2 (purple), O_3 (green), (b) photolysis rate (blue), and NO_2/NO_x ratio (black) over inland region.

doi:10.6342/NTU202201146

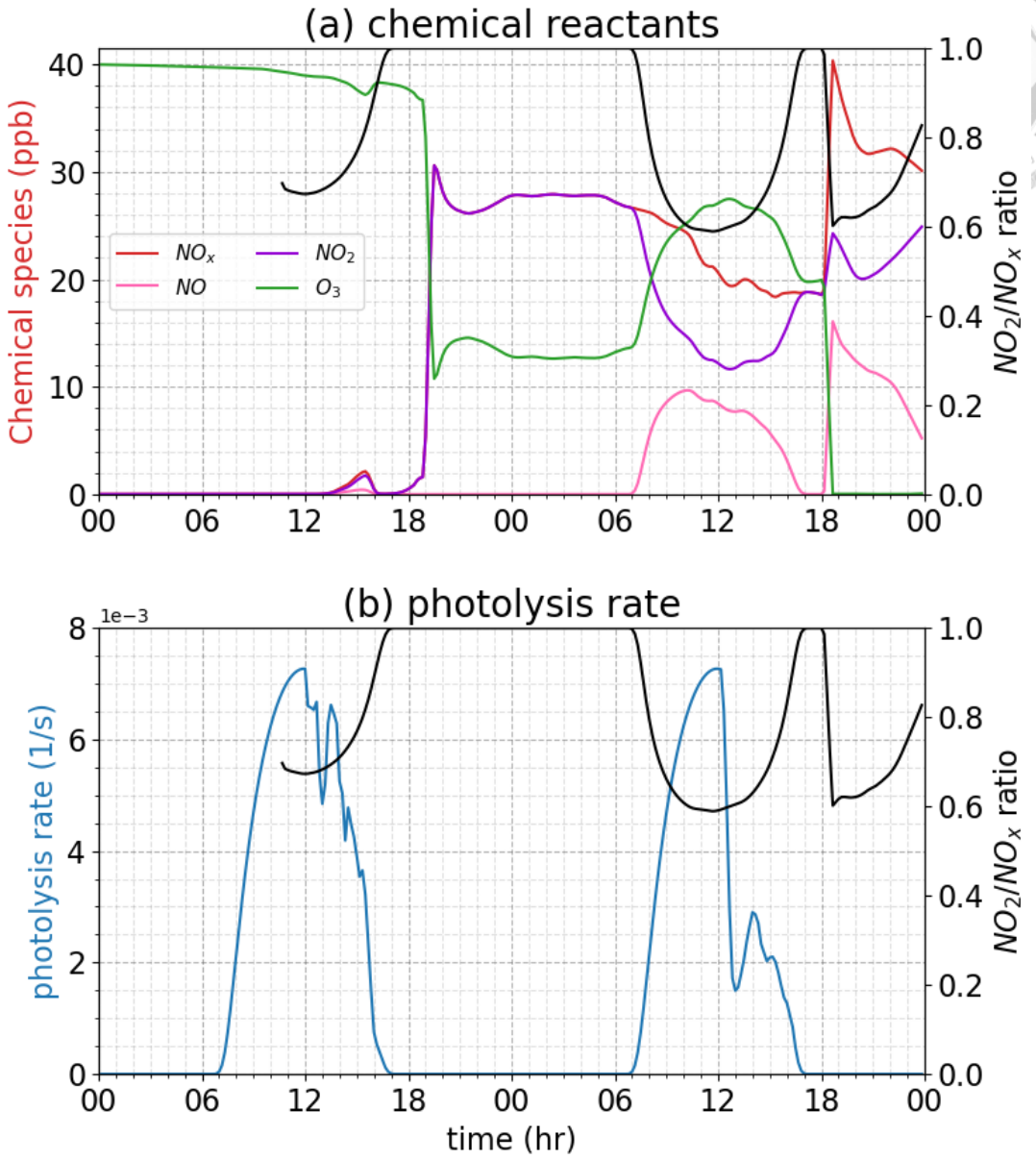

Fig. 16: Time evolution of (a) NO_x (red), NO (pink), NO_2 (purple), O_3 (green), (b) photolysis rate (blue), and NO_2/NO_x ratio (black) over hillside region.

doi:10.6342/NTU202201146

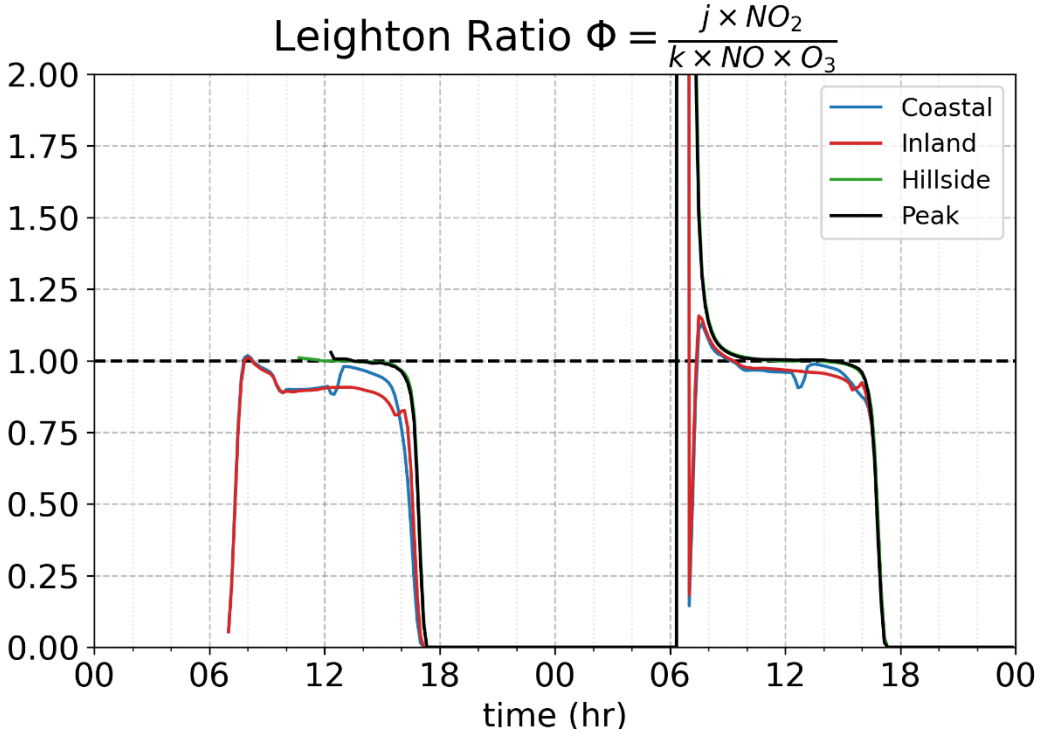

Fig. 17: Time evolution of Leighton ratio over coastal (blue), inland (red), hillside (green), and peak (black) regions.

doi:10.6342/NTU202201146